## **All-atom Modeling of Complex Cellular Membranes**

Min-Kang Hsieh, 1,† Yalun Yu, 2,† and Jeffery B. Klauda 1,2\*

<sup>1</sup>Department of Chemical and Biomolecular Engineering, <sup>2</sup>Biophysics Graduate Program University of Maryland,
College Park, MD 20742, USA

\*Corresponding Author: <u>jbklauda@umd.edu</u>
†Contributed equally to this Article (co-first authors)

#### **Abstract**

Cell membranes are composed of a variety of lipids and proteins where they interact with each other to fulfill their roles. The first step to model these interactions in molecular simulations is to have reliable mimetics of the membrane's lipid environment. This *Feature Article* presents our recent efforts to model complex cellular membranes using all-atom force fields. A short review of the CHARMM36 (C36) lipid force field and its recent update to incorporate the long-range dispersion is presented. Key examples on model membranes mimicking various species and organelles are given. These include single-celled organisms like bacteria (*E. coli.*, chlamydia, and *P. aeruginosa*) and yeast (plasma membrane, endoplasmic reticulum, and trans-Golgi network) and more advanced ones such as plants (soybean and *Arabidopsis thaliana*) and mammals (ocular lens, *stratum corneum*, and peripheral nerve myelin). Leaflet asymmetry in composition has also been applied to some of these models. With the increased lipid diversity in the C36 lipid FF, these complex models can better reflect the structural, mechanical, and dynamic properties of realistic membranes and open an opportunity to study biological processes involving other molecules.

#### Introduction

The cell membrane is a complex mixture of lipids and proteins that can provide protection to the cell as a plasma membrane (PM) or define cellular organelles, e.g., endoplasmic reticulum (ER), trans-Golgi Network (TGN), and mitochondria.<sup>1</sup> Although membrane-associated proteins have been a strong focus in research on cell signaling,<sup>2-4</sup> molecular transport across cell membranes,<sup>5-8</sup> and shuttles for lipid movement within/between organelles,<sup>9-13</sup> proteins do not reside in a homogenous sea of lipids that form a bilayer. These cellular membranes are quite dynamic and can have hundreds of varied lipids that can phase separate into liquid ordered and disordered domains.<sup>1, 14, 15</sup> These varied domains within a given organelle are believed to be important to certain functions of membrane-associated proteins. Ultimately, it is important to fully investigate the physical properties of cellular membranes to provide insight into an organelle's evolved lipid composition or specifics to membrane-protein interaction.

Key to understand the physical properties of realistic cellular membranes is obtaining the lipid composition of cells and organelles. <sup>16-22</sup> Original studies were on overall lipid compositions of entire cells like that done for yeast with mass spectroscopy. <sup>16</sup> Experimental techniques to pull out individual organelles of the cell allow for improved quantification of cellular distribution of lipids. <sup>17</sup> More recent lipidomic studies with enhanced resolution can provide detailed distributions of head groups and associated tails. <sup>16</sup> Moreover, cell membrane leaflets for many organelles are known to consist of varied concentrations of lipid head groups and acyl chains. <sup>1, 18</sup> This was first quantified through biochemical studies (enzymatic modification, chemical modification, lipid exchange and physiochemical techniques) on a red blood cell (RBC) because it lacks organelles. <sup>18, 19</sup> More recently, Lorent et al. <sup>20</sup> extended past work on RBCs by enzymatic lipid removal and mass spectroscopy of 400 lipid species to quantify the head groups and acyl chains. The inner leaflet was shown to have approximately twofold more unsaturated when compared to the outer leaflet.

The focus of this *Feature Article* is using computational modeling to probe cell membrane physical properties. Key to developing models and simulating the natural movement of lipids, is an accurate mathematical description of interactions between molecules. Once this is obtained, then Newton's Second Law,  $F = m \cdot a$  (force equals mass times acceleration), can be solved using the functional form for the force, known as a force field. With experimental lipidomic studies, models of cellular membrane can be developed. Tools, such as CHARMM-GUI's *Membrane Builder*<sup>23-26</sup> and Insane<sup>27</sup>, have made the hard task building of complex cellular membranes more straightforward. Moreover, with increasing computational power, the ability to probe membranes with 5 or more lipid types that properly sample configurational space has made the study of realistic cellular membranes feasible.

This *Feature Article* will focus on our lab's efforts in the field of cell membrane modeling and is not an exhaustive review of work from other labs, which can be found in other works.<sup>28-30</sup> First, the development of accurate all-atom lipid force fields will be described and how these are key toward accurate modeling of cellular membranes. The second section will summarize our work on modeling bacterial membranes from the simple cytoplasmic membrane in gram-negative bacteria to the more complex outer membrane. Membrane modeling of a more complex single-celled organism, i.e., yeast, will be presented in the third section. Then, the fourth section presents our efforts in modeling plant membranes and the last section recaps some initial efforts toward modeling mammalian membranes.

## Importance of Accurate All-Atom Lipid Force Fields

Introduction to Force Fields. Molecular simulations provide detailed information of the structure and dynamics of biological systems with proteins, lipids, sugars, and nucleic acids. A crucial part of the simulation is the force field (FF), which is the potential energy function to describe the interaction within the simulated system. In this *Feature Article*, we focus on the lipid FFs. <sup>31-47</sup> Lipid molecules are amphiphilic with a hydrophilic head and hydrophobic tails, which enables them to act as a barrier between different biological environments where specific chemical reactions may happen to increase biochemical efficiency and restrict dissemination of reaction products. The development of a lipid FF is either targeted at the two major segments<sup>32, 48</sup> or at smaller residues for each segment. <sup>37, 49</sup> The parameterization procedure is usually a combination of theoretical calculations such as quantum mechanics (QM) and empirical adjustments using molecular dynamics (MD) simulations. Based on the modeling strategy, popular lipid FFs can be divided into four major groups - additive atomistic FFs, polarizable FFs, united-atom (UA) FFs, and coarse-grained FFs. The parameters associated with these FFs are harmonic bonded terms, dihedral terms, and nonbonded terms (electrostatics and van der Waals). In atomistic FFs, 31-37 all atoms including hydrogens are assigned a mass and its own nonbonded parameters. Polarizable FFs can also model the induced dipoles for all the atoms in the system<sup>38</sup> or the heavy atoms.<sup>39,40</sup> In a UA FF, selected hydrogens are lumped into their bonded heavy atoms forming the united atoms, 41-45 so that the total mass and the effective nonbonded parameters are used for each united atom. For coarse-grained FFs, multiple heavy atoms are grouped together. 46, 47 For more details about these FFs, please refer to the review article by Leonard et al.<sup>28</sup> The choice of the lipid FF in simulations depends on the trade-off between efficiency and accuracy, the type of problem being solved, the compatibility with the non-lipid part of the simulated system and more.

CHARMM36 and Diversity. The potential energy for the all-atom CHARMM36 lipid FF can be written as

$$V(\hat{R}) = \sum_{\text{bonds}} K_{b,ij} (r_{ij} - r_{0,ij})^{2} + \sum_{\text{angles}} K_{\theta,ijk} (\theta_{ijk} - \theta_{0,ijk})^{2}$$

$$+ \sum_{\text{Urey-Bradley}} K_{ub,i(i+2)} (r_{i(i+2)} - r_{0,i(i+2)})^{2} + \sum_{\text{improper}} K_{\phi,ijkl} (\phi_{ijkl} - \phi_{0,ijkl})^{2}$$

$$+ \sum_{\text{dihedrals}} \sum_{n} K_{\phi,n} (1 + \cos(n\phi_{ijkl} - \delta_{n}))$$

$$+ \sum_{\text{nonbonded pairs}} \varepsilon_{ij} \left[ \left( \frac{R_{\min,ij}}{r_{ij}} \right)^{12} - 2 \left( \frac{R_{\min,ij}}{r_{ij}} \right)^{6} \right] + \sum_{\text{electrostatic}} \frac{q_{i}q_{j}}{4\varepsilon_{0}r_{ij}}$$

$$(1)$$

where r is the distance between two atoms,  $\theta$  is the angle formed by three atoms,  $\phi$  is the improper angle,  $\varphi$  is the dihedral angle,  $\delta_n$  is the phase shift for multiplicity n. In the CHARMM FF, a minimal number of dihedral terms is used to best represent the torsional profile, though the multiplicity can vary from 1 to 6. For the van der Waals interaction, CHARMM uses the Lennard-Jones (LJ) potential where  $R_{\min}$  is the distance at which the LJ potential (of a specific atom pair) reaches its minimum. The electrostatic interaction follows Coulomb's Law where q is particle charge of atoms and  $\varepsilon_0$  is vacuum permittivity.

The CHARMM36 (C36) lipid FF uses the particle-mesh Ewald (PME) method<sup>50</sup> for the electrostatic interactions and a force-based switching function ranging from 8 to 12 Å for the LJ. This treatment for the LJ interactions was needed at the time of parameterization since there was no efficient algorithm for the long-range dispersion. However, the nonbonded terms, especially the electrostatic parameters, were carefully optimized to match surface area per lipid  $(A_{lip})$  for a 1,2-dipalmitoyl-sn-glycero-3-phosphocholine (DPPC) bilayer and the aqueous solvation free energies of methylacetate (MAS) and dimethylphosphate (DMP). The initial parameterization focused on DPPC but was also tested against 1-palmitoyl-2-oleoyl-snglycero-3-phosphoethanolamine (POPE), which is a monounsaturated lipid. The agreement with experimental  $A_{\rm lip}$  and head group structure (measured by the deuterium order parameters,  $S_{\rm CD}$ ) for these lipids was outstanding. However, the isotherm of lipid monolayer  $A_{\rm lip}$  versus surface tension was not accurately modeled by this FF due to the lack of long-range dispersion. In the following years, more lipid head groups were added to the FF. These include a systematic parameterization of the non-bonded fix (NBFIX) terms between ions and the ester and carbonyl oxygens to incorporate phosphatidylglycerol (PG) and phosphatidylserine (PS) lipids, and the extensive tests on phosphatic acids (PA)<sup>51</sup> and phosphatidylinositols (PI).<sup>52</sup> Sphingolipids and ceramides have been parameterized and tested in a series of studies. 53-55 Following the re-optimization of the ether linkage to increase bilayer hydration, 56 parameters for plasmalogens (which contain a vinyl-ether and an ester bond at the sn-1 and sn-2 positions, respectively) were developed recently.<sup>57</sup> Glycolipids and lipopolysaccharides (LPS) have also been developed and tested<sup>58-61</sup> utilizing the CHARMM carbohydrate FF. <sup>62-65</sup> Aside from this head group diversity, work has also

been focused on the varying lipid tails, i.e., polyunsaturated,<sup>66</sup> branched,<sup>67</sup> and cyclic-containing.<sup>68, 69</sup> The C36 lipid FF also supports various sterols.<sup>70-72</sup>

CHARMM36 LJ/PME. Long-range dispersion has been excluded from the potential energy in most FFs due to its relatively fast decay ( $\propto r^{-6}$  compared to  $\propto r^{-1}$  for electrostatics). This is a reasonable treatment when the electrostatic interactions are dominant for the simulated system (for example, a water box) or when the properties of interest are not sensitive to the long-range dispersion.<sup>73</sup> However, as mentioned in the previous section, the lack of long-range dispersion in the C36 lipid FF leads to the inconsistency between bilayers and monolayers. This is because the acyl chain/air interface in a monolayer system requires the long-range dispersion to reproduce experiment as indicated by studies using alkanes. 74-76 This inconsistency was recently resolved by a re-parameterization 77, 78 of the FF focusing on the ester and ether linkages to incorporate the long-range dispersion explicitly through the LJ particle-mesh Ewald (LJ-PME) method. The new FF was named C36/LJ-PME. Parameters for the acyl chain were not changed in this reparameterization since they already produce accurate densities of alkanes for a wide range of temperatures when using LJ-PME.<sup>74</sup> It should be noted that there are alternative approaches to compensate for the longrange dispersion such as the analytic long-range correction (LRC)<sup>32</sup> and the pressure-based LRC.<sup>79</sup> However, LJ-PME is more rigorous and suitable for heterogeneous systems such as lipid bilayers and monolayers. Another benefit of C36/LJ-PME is the elimination of the LJ cutoff, which means the lipid FF can be used with other FFs parameterized with the long-range dispersion or ones that are not sensitive to the cutoff, such as a protein FF.<sup>73</sup>

The parameterization of C36/LJ-PME initially focused on the PC head group and the ether linkage, and validation of the FF was extended to PE and PG lipids. Bilayers and monolayers simulated with C36/LJ-PME showed good agreement with experimental structure data (scattering data and NMR deuterium order parameter) and NMR  $T_1$  relaxation times for varying carbon positions (both head group and acyl chain). An example of such a comparison is in Figure 1 where the  $A_{\rm lip}$ , head-to-head thickness (D<sub>HH</sub>), and monolayer surface tension compare favorably with experiment. However, lipid diffusion derived for the infinite system size is too fast (almost two-fold) compared to experiment. A semi-automated approach was used for this re-parameterization, which utilized thermodynamic reweighting to estimate the property sensitivity, and the change of parameter in each iteration was determined in a least-square manner. Parameter restraints were also added to the residual function to keep C36/LJ-PME close to C36. This approach greatly reduced the time needed to re-parameterize the FF and the whole parameterization took only a couple of months. However, there are pitfalls with such an automated method such as overfitting and sampling issues, and more about these problems were discussed in the original publication<sup>77</sup> and a recent review.<sup>80</sup>

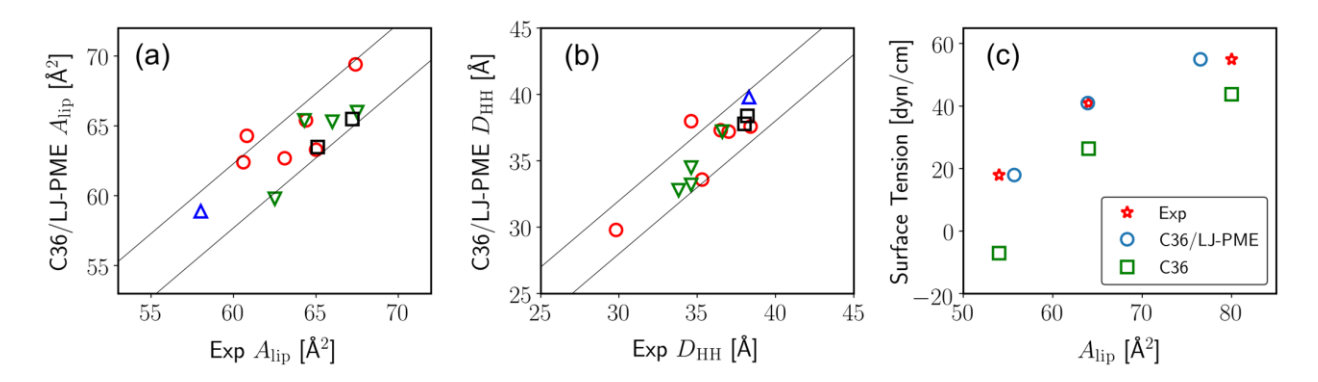


**Figure 1.** Area per lipid,  $A_{\text{lip}}$  (a) and head-to-head distance,  $D_{\text{HH}}$  (b) obtained from C36/LJ-PME simulation compared with experiment (Exp). Red circles are PC lipids, green upside-down triangles are PG lipids, blue triangles are PE lipids, black squares are ether lipids. Black diagonal lines represent the 95% confidence intervals of the experimental measurements. (c) Surface tension vs.  $A_{\text{lip}}$  for DPPC monolayer obtained from simulation (C36/LJ-PME and C36) compared with experiment (Exp).

To keep consistency with the other parts of the CHARMM FF, the TIP3P water model<sup>81,82</sup> was used in C36/LJ-PME. The addition of the long-range dispersion has negligible influence on the solvent-solvent and solvent-solute interactions since they are dominated by electrostatics, and this can be demonstrated by the radial distribution functions (RDFs) between water and lipid atoms, which remained unchanged when the long-range dispersion was added.<sup>77</sup> However, there are known flaws of the TIP3P water model such as the too-fast diffusion and the failure to reproduce local structures accurately, though these are unavoidable for a three-point additive water model. While further development of C36/LJ-PME to incorporate more lipids is necessary, a better polarizable lipid FF with a better water model is in urgent need. Currently, popular simulation programs compatible with C36/LJ-PME are GROMACs,<sup>83,84</sup> CHARMM,<sup>74,85</sup> and OpenMM.<sup>86</sup>

## **Summary of Membrane Properties Covered by this Review**

The following sections of this *Feature Article* will focus on our lab's efforts in various biological membrane models. In the Bacterial Membrane Modeling section, the inner membrane (IM) of *E. coli*, *Chlamydia trachomatis*, and *P. aeruginosa* and the outer membrane (OM) of *E. coli* will be described. Yeast-like membrane models and yeast organelle membrane models for the ER, TGN, and the PM will be presented in Yeast Membrane Models section. The Plant Membrane will present the PM of soybean and *A. thaliana*. Ocular lens, Stratum Corneum, and Peripheral nerve myelin modeled membranes will be descried in the Mammalian Membrane Models section. Table 1 summarizes the important membrane properties, i.e., surface area per lipid ( $A_{lip}$ ), the head-to-head thickness ( $D_{HH}$ ), the overall bilayer thickness ( $D_B$ ), the

hydrophobic core thickness  $(2D_C)$ , and the area compressibility modulus  $(K_A)$  of all membrane models presented in this work. The detail of models and other membrane properties can be found in the original reports.

Table 1. Membrane Properties for Each Model. <sup>a</sup>

Model	A <sub>lip</sub> (Å <sup>2</sup> )	$D_{ m HH}({ m \AA}^2)$	$D_{\mathrm{B}}(\mathring{\mathrm{A}}^{2})$	2D <sub>C</sub> (Å <sup>2</sup> )	K <sub>A</sub> (N/m)
Bacterial Membrane					
E. coli IM Top6 <sup>68</sup>	$64 \pm 1$		$37.3 \pm 0.2$	$29.8 \pm 0.1$	$0.34 \pm 0.04$
E. coli IM early-log 101	$60.77\pm0.02$	$37.73 \pm 0.13$	$38.27 \pm 0.12$	$30.62\pm0.13$	$0.28 \pm 0.02$
E. coli IM mid-log 101	$61.26\pm0.04$	$38.00 \pm 0.11$	$38.15 \pm 0.03$	$30.36\pm0.03$	$0.29 \pm 0.01$
E. coli IM stationary 101	$62.48 \pm 0.07$	$37.33 \pm 0.07$	$37.07 \pm 0.07$	$30.00\pm0.03$	$0.31 \pm 0.01$
E. coli IM overnight 101	$63.08\pm0.17$	$37.00 \pm 0.23$	$36.82 \pm 0.10$	$30.09 \pm 0.13$	$0.33 \pm 0.03$
E. coli IM early-log (asym) 103	$60.86 \pm 0.08^{b}  62.46 \pm 0.08^{c}$	$39.07\pm0.22$	$38.04 \pm 0.06$	$28.96 \pm 0.04$	$0.26 \pm 0.01$
E. coli IM stationary (asym) 103	$62.41 \pm 0.09^b  64.05 \pm 0.10^c$	$38.53 \pm 0.16$	$37.13 \pm 0.09$	$28.66 \pm 0.04$	$0.29 \pm 0.01$
Chlamydia EB <sup>67</sup>	$47.14 \pm 0.06$	44.1			$0.583\pm0.081$
Chlamydia RB <sup>67</sup>	$49.45\pm0.06$	42.3			$0.459\pm0.007$
P. Aeruginosa IM Planktonic 69	$61.19 \pm 0.25$	$41.1 \pm 0.2$	$39.9 \pm 0.2$	$30.4 \pm 0.1$	$0.28 \pm 0.02$
P. Aeruginosa IM Biofilm <sup>69</sup>	$61.20\pm0.22$	$40.3 \pm 0.1$	$38.9 \pm 0.3$	$29.7 \pm 0.3$	$0.23\pm0.02$
E. coli OM LPS-PL[36,100] <sup>58</sup>	$182\pm1^{\rm d}$			24.7	
E. coli OM LPS-PL[37,100] <sup>58</sup>	$177\pm03^{\rm d}$			24.8	
Yeast Membrane					
Yeast CPRΔ1 <sup>23</sup>	$51.6 \pm 0.2$	$43.0 \pm 0.1$			
yeast CPR∆1 sat <sup>23</sup>	$44.6 \pm 0.1$	$46.8 \pm 0.6$			
yeast CPR $\Delta$ 1 sat - $\gamma$ 10 <sup>23</sup>	$47.2\pm0.3$	$45.8 \pm 0.6$			
yeast hypo <sup>23</sup>	$48.8 \pm 0.2$	$45.2 \pm 0.8$			
yeast ER1 <sup>71</sup>	$64.0 \pm 0.4$	$37.8 \pm 0.1$	$34.4 \pm 0.2$	$29.1 \pm 0.2$	$0.29 \pm 0.02$
yeast ER2 <sup>71</sup>	$63.6 \pm 0.4$	$37.4 \pm 0.1$	$34.1 \pm 0.2$	$29.3 \pm 0.2$	$0.28 \pm 0.02$
yeast TGN1 <sup>71</sup>	$60.6 \pm 0.4$	$38.6 \pm 0.1$	$36.4 \pm 0.2$	$26.5 \pm 0.2$	$0.28 \pm 0.06$
yeast TGN2 <sup>71</sup>	$60.9 \pm 0.4$	$38.4 \pm 0.1$	$35.8 \pm 0.2$	$29.7 \pm 0.2$	$0.27 \pm 0.02$
yeast PM1 <sup>71</sup>	$47.4 \pm 0.2$	$43.4 \pm 0.1$	$39.3 \pm 0.2$	$34.4 \pm 0.2$	$0.57 \pm 0.06$
yeast PM2 <sup>71</sup>	$46.8\pm0.3$	$44.4 \pm 0.1$	$39.6 {\pm}~0.2$	$34.9 \pm 0.2$	$0.47 \pm 0.08$
AVG-yeast <sup>71</sup>	$47.3\pm0.3$	$43.0 \pm 0.1$	$39.9 \pm 0.2$	$34.0 \pm 0.2$	$0.34 \pm 0.04$
Plant Membrane					
Soybean PM hypocotyl <sup>72</sup>	$52.7 \pm 0.2$	$42.7 \pm 0.3$	$40.1 \pm 0.1$	$32.0 \pm 0.1$	$0.51 \pm 0.07$
Soybean PM root <sup>72</sup>	$51.9 \pm 0.1$	$42.7 \pm 0.1$	$39.3 \pm 0.1$	$32.2 \pm 0.04$	$0.57 \pm 0.06$
A. thaliana PM plant 1 <sup>138</sup>	$43.66 \pm 0.03^b  48.03 \pm 0.03^c$				
A. thaliana PM plant 2 <sup>138</sup>	$42.53 \pm 0.04^b  47.50 \pm 0.04^c$	$43.6 \pm 0.4^e$	$40.8 \pm 0.2^{\text{e}}$	$34.3 \pm 0.1^{\text{e}}$	$0.94 \pm 0.04^{\text{e}}$
A. thaliana PM plant 3 <sup>138</sup>	$43.67 \pm 0.04^b  48.03 \pm 0.04^c$				
Ocular Lens <sup>144</sup>					
PC:NSM	$57.7 \pm 0.2$	$43.40\pm0.00$	$45.36 \pm 0.12$	$33.63 \pm 0.04$	

PE:NSM	$58.5 \pm 0.1$	$45.00\pm0.14$	$45.39 \pm 0.02$	$35.01\pm0.04$	
PC:NSM:CHOL	$39.58 \pm 0.03$	$47.80 \pm 0.14$	$41.06\pm0.01$	$36.17 \pm 0.01$	
PC:DHSM:CHOL	$39.44\pm0.03$	$47.20\pm0.10$	$41.41\pm0.04$	$36.25\pm0.02$	
PE:NSM:CHOL	$40.79\pm0.03$	$46.60\pm0.14$	$40.95\pm0.01$	$36.10 \pm 0.01$	
PE:DHSM:CHOL	$40.70\pm0.03$	$46.73\pm0.14$	$41.12 \pm 0.05$	$36.22\pm0.04$	
PE:PC:NSM:CHOL	$40.35\pm0.03$	$46.73\pm0.14$	$41.12 \pm 0.05$	$36.22 \pm 0.04$	
PE:PC:DHSM:CHOL	$40.40\pm0.03$	$46.13\pm0.05$	$40.52\pm0.10$	$35.56 \pm 0.04$	
Stratum Corneum Models <sup>146</sup>					
CerNS/Chol/LA X <sub>CER</sub> =0.20	$31.18 \pm 0.02$	$48.9 \pm 0.2$	$48.07\pm0.02$	$43.62\pm0.03$	$3.9 \pm 0.1$
CerNS/Chol/LA X <sub>CER</sub> =0.34	$32.81\pm0.01$	$49.1 \pm 0.1$	$50.27\pm0.03$	$44.4 \pm 0.1$	$3.4 \pm 0.1$
CerNS/Chol/LA X <sub>CER</sub> =0.50	$34.50\pm0.08$	$49.9 \pm 0.2$	$52.7 \pm 0.1$	$45.33\pm0.03$	$3.78 \pm 0.06$
CerNS/Chol/LA X <sub>CER</sub> =0.70	$36.79\pm0.03$	$51.1\pm0.5$	$54.72 \pm 0.02$	$46.4 \pm 0.1$	$3.26\pm0.03$
CerAP/Chol/LA X <sub>CER</sub> =0.20	$31.18 \pm 0.08$	$47.9 \pm 0.2$	$48.4 \pm 0.1$	$43.16 \pm 0.04$	$3.9 \pm 0.2$
CerAP/Chol/LA X <sub>CER</sub> =0.34	$32.62\pm0.07$	$48.6 \pm 0.1$	$51.2 \pm 0.2$	$43.98 \pm 0.04$	$4.5 \pm 0.2$
CerAP/Chol/LA X <sub>CER</sub> =0.50	$34.53\pm0.04$	$49.6 \pm 0.1$	$53.3 \pm 0.2$	$44.87 \pm 0.01$	$4.2 \pm 0.4$
CerAP/Chol/LA X <sub>CER</sub> =0.70	$37.41\pm0.06$	$50.2 \pm 0.1$	$54.55\pm0.01$	$45.6 \pm 0.1$	$3.3 \pm 0.1$
CerNS/Chol/LAP X <sub>CER</sub> =0.34	$32.63 \pm 0.0$	$49.7 \pm 0.2$	$51.4 \pm 0.1$	$44.7 \pm 0.1$	$4\ 3.7\pm0.1$
Peripheral Nerve Myelin 147					
PI-containing, nondiabetic	$47.66\pm0.12$	$43.3 \pm 0.2$	$42.4 \pm 0.0$	$32.9 \pm 0.0$	$0.42\pm0.03$
PS-containing, nondiabetic	$48.24\pm0.08$	$43.5 \pm 0.2$	$41.2 \pm 0.1$	$32.8 \pm 0.0$	$0.45\pm0.02$
PI-containing, diabetic	$58.51\pm0.24$	$39.7 \pm 0.1$	$40.0 \pm 0.2$	$30.1\pm0.1$	$0.20 \pm 0.01$
PS-containing, diabetic	$59.08\pm0.37$	$40.1\pm0.1$	$38.8 \pm 0.2$	$30.0 \pm 0.1$	$0.19 \pm 0.01$

<sup>&</sup>lt;sup>a</sup> Values are reported with the standard errors from the original article; the blank is shown if the value was not reported.

# **Bacterial Membrane Modeling**

Bacteria offer a good starting point for membrane modeling because the diversity of lipids is reduced compared to eukaryotes. Traditionally, model membranes of bacteria were limited to two-component phospholipid (PL) mixtures of phosphoethanolamine (PE) and PG in simulation<sup>87-94</sup> and experiment.<sup>95-100</sup> However, bacteria are known to produce lipids with varied acyl chain types. This section describes our efforts to model the inner and outer membranes of various bacteria. Our lab has developed advanced lipid bilayer models with accurate lipid diversity and leaflet asymmetry in compositions to reflect the realistic complexity of membranes that mimic the bacterial membranes. Models for the *E. coli* cytoplasmic

 $<sup>^{\</sup>rm b}$  The  $A_{\rm lip}$  of the outer leaflet of the asymmetric membrane is reported.

 $<sup>^{\</sup>rm c}$  The  $A_{\rm lip}$  of the inner leaflet of the asymmetric membrane is reported.

<sup>&</sup>lt;sup>d</sup> The surface area per Lipid A is reported.

<sup>&</sup>lt;sup>e</sup> The average from the three *A. thaliana* PM membranes is reported.

membrane or inner membrane (IM) constitutes PE and PG lipids in general with a cyclopropane ring in the fatty tail of lipids that increases in concentration from the early to the end of the bacterial lifecycle.<sup>68, 101</sup> Another gram-negative bacteria IM model, *Pseudomonas aeruginosa*, was developed for two states, biofilm and planktonic, in which the former is more resistant to environmental stress compared to the latter.<sup>69</sup> While *E. coli* has acyl chains with cyclopropane moieties, we have also done modeling for *Chlamydia trachomatis*, containing methyl branches at the iso- and anteiso-positions of lipid tails focusing on its biphasic life cycle (elementary body, which enters and infects the host cell initially, and the reticular body, which metabolically more active).<sup>67</sup> We also discuss our modeling of the asymmetric leaflet in lipid compositions for the well-known OM of *E. coli*<sup>58, 60, 102</sup> and also the less understood IM.<sup>103</sup>

Cytoplasmic Membrane of E. Coli. Bacterial inner membranes have been observed to consist of 70~80% PE, 10-20% PG and < 10% cardiolipin lipid (CL) from the experimental measurements. <sup>104-107</sup> Initial membrane modeling typically consisted of a simplified two-component POPE/POPG bilayer. 87-89 CL distributes in the polar and septal regions to induce curvature<sup>97, 108, 109</sup> and is typically not included in typical IM bacterial bilayer models. These models match the main compositions of lipid head groups but ignore the lesser-known diversity of lipid tails. Pandit and Klauda<sup>68</sup> were the first to develop IM models that considered the presence of a cyclic moiety in lipid tails. Quantum mechanics was used to develop dihedral potentials of the cyclopropane moiety of the 1-palmitoyl-2-cis-9,10-methylene-hexadecanoic-acid-snglycero-3-phosphoethanolamine (PMPE) lipid. Bilayer simulations of PMPE resulted in excellent agreement with the deuterium NMR experiment for the S<sub>CD</sub> of the cyC19:0 acyl chain of l-palmitoyl-2-dihydrosterculoyl-sn-glycero-3-phosphoethanolamine (PDSPE) lipid. Consequently, these parameters were then used in simulations of a complex bacterial IM model of six lipid types (Top6 model) to represent the K12 CSH2 E. coli. The membrane model was developed with a 4.2 PE:PG ratio and included various fatty acid tails of 15:0, 16:0, 16:1, 18:1, and cyC17:0 in 7%, 40%, 8%, 10%, and 35%, respectively. The Top6 model (identified as the overnight stage or the death stage) revealed that the bilayer is thinner and has less surface density and greater area compressibility modulus (KA) compared to the simple POPE/POPG membrane. The Top6 membrane also matched the hydrophobic length of known integral E. coli membrane protein better.

To further our understanding of the IM of *E. coli*, the effect of lipid composition changes during the life cycle of *E. coli* on bilayer properties was probed. The models emphasized an increase in the percentage of lipids with cyC17:0 acyl chain at 0%, 18%, 53%, and 70% representing the earlylog, midlog, stationary, and overnight stages, respectively. This focused on *E. coli*'s two different regimes in its chronological development: the growth stages (earlylog and midlog) and the plateau stages (stationary and overnight). The membrane becomes less dense, lower chain order, and thinner from the growth stages to

the plateau stages. It also revealed that the  $A_{lip}$  increases among lipids with cyC17:0 tails. Lipid diversity of complex  $E.\ coli$  IM models provides more accurate membrane properties with detailed molecular structural information during the developmental cycle of the bacterium and allows for studies on various applications such as studies of antibiotic transport across the IM or passive movement of ethanol across the IM.

One such example application was our work that investigated the effects of engineering E. coli membrane with a strain-specified lipid concentration in our collaboration with the Jarboe group at Iowa State University. The this work, the membrane modeling assisted to probe the impact of microbial membrane during a production of biorenewables. Bacterial membranes were constructed to match the lipid composition measurements of the evolved strain, as well as the control and exchange of the head group and tail of these two bacterial strains (hybrid models) for examining their impact on membrane properties." These models were used to study membrane integrity (and permeability) by analyzing the surface density, thickness, order parameter, and  $K_A$ . In water solvent, the head-to-head thickness of the PE-enriched (+pssA model) bilayer was larger than the control bilayer. In the presence of ~4.5 mol% ethanol solvent to simulate a microbial production environment, the  $A_{lip}$  was higher in both models. The thicknesses significantly decrease in both models, except for the insignificant change in the hydrophobic core thickness of +pssA model, that indicated its resistance to permeation by ethanol. The evidence of the upper chain order parameter and electron density profile of the phosphate and carbonyl groups also concluded that the PE-enriched E. coli IM membranes improve their tolerance in the ethanol solvent.

Beyond lipid diversity, leaflet asymmetry in lipid compositions for the *E. coli* IM has been recently developed to consider its effect on lipid properties <sup>103</sup> and influence on TM protein orientation due to the positive inside rule. <sup>111</sup> The leaflet asymmetry reflecting the natural heterogeneous lipid mixture of cellular bilayers has been found in the cytoplasmic membrane of eukaryote on the local membrane region, so that, many studies are interested in remodel the asymmetric membrane and examination involving biological activities. <sup>112-116</sup> However, asymmetry in the bacterial IM has also been hypothesized without direct lipidomics on leaflets due to the challenge of the experimental measurement. Leaflet asymmetric *E. coli* IM models of the earlylog and stationary stages have been constructed with a more negative-charged lipids (PG) on the inner leaflet than the outer leaflet, in which the PE/PG ratio was set to 2.8 and 6.8, respectively. The percentages of lipids with cyC17:0 acyl chain were at 0 and 51% in earlylog and stationary stage, respectively. During the chronological development of *E. coli*, like the previous probe in the four stages modeling, the similar results showed that the surface density was less, the thickness was thinner, and the deuterium order parameters were lower in the plateau stages, compared to the growth stages. Examining the asymmetric distribution of lipid composition across the leaflets showed less surface density, thinner, and more tilt and disordered lipid tails at the inner leaflet than the outer leaflet in both stages. While the

 $A_{\rm lip}$ , leaflet thickness, and tilt angle of hydrophobic tails act correspondingly by assuming a roughly constant leaflet volume, the deviation of these leaflet properties from the reference membranes (symmetric models) depends on the containing lipid components. Our simulations suggest that membrane properties in the asymmetric models are more dependent on the percentage of PG compared to the symmetric models. In our perspective, the leaflet asymmetry and lipid diversity with an appropriate mixture of various lipid types reflect a more realistic membrane that will provide a more accurate representation of the interaction, structure, and dynamics of membrane-associated molecules and orientation of membrane-associated proteins.

Chlamydia. Early in our lab's membrane modeling efforts, the cytoplasmic membrane of Chlamydia trachomatis was studied to probe the bacterium biphasic life cycle of the elementary body (EB) and the reticular body (RB) stages.<sup>67</sup> The EB is a small cell type and occupies the host cell at the initial infection, whereas the RB is a larger cell type and metabolically active in the host cell. The mainly constituted methyl benched lipids results in highly stable bacterial bilayer and low permeability to water. <sup>117, 118</sup> Initial modeling was performed with various PC lipids with methyl branches at iso- and anteiso-positions, including 1-13methylpen-tadecanoyl-2-palmitoyl-phosphatidylcholine 1-14-methylpentadecanoyl-2-(13-MpPPC), palmitoyl-phosphatidylcholine (14-MpPPC) and diphytanoylphosphatidylcholine (DPhPC, methyl branches at the 3, 7, 11, and 15 positions in both fatty acid tails) that compared favorably with experimental measures. Briefly, the simulated  $A_{lip}$  of 13-MpPPC, 14-MpPPC, and DPPC bilayer were  $63.8 \pm 0.2 \text{ Å}^2$ , 62.9 $\pm$  0.2 Å<sup>2</sup>, 62.9  $\pm$  0.3 Å<sup>2</sup>, agreeing with the experiment  $A_{lip}$  of DPPC (63  $\pm$  1.0 Å<sup>2</sup>). The calculated  $A_{lip}$  of DPhPC were  $76.1 \pm 0.1 \text{ Å}^2$  (298K) and  $80.5 \pm 0.1 \text{ Å}^2$  (323K), matching the measured  $A_{\text{lip}}$  76 Å<sup>2</sup> (298 K) and  $80.5 \pm 1.5 \text{ Å}^2$  (303.15K). The EDP has a very similar shape in both model and experiment of DPhPC bilayer and its peak-to-peak distance was 37.6 Å (calculation) and 36.4 Å (experiment); the average peak density was 0.428 e/Å<sup>3</sup> (calculation) and 0.429 e/Å<sup>3</sup> (experiment). The details of validation of methyl branches lipid membrane could be found in the original article.<sup>67</sup> Therefore, we developed a model for this bacteria with a total of 9 lipid types containing PC, PE, PG, Chol at 28.8%, 34.4%, 3.2%, and 33.6% for EB and 32.8%, 36.8%, 4.8%, and 25.6% for RB as well as variations in the acyl chains to match the experimental data. 119 The simulations used the updated C36 FF<sup>67</sup> for the branched-chain topology. The result revealed that membranes containing lipids with methyl branches tend to increase lipid  $A_{\rm lip}$ , decrease chain order, increase  $K_A$ , and increase lipid axial relaxation times. The  $K_A$  is different between EB and RB models. The higher moduli in EBs leads to a greater membrane stiffness, which we hypothesize makes it easier to penetrate host cells and less permeable to solutes as a metabolically inactive form.

Inner Membrane of *Pseudomonas Aeruginosa*. Aside from *E. coli*, we have also studied the cytoplasmic membrane of another gram-negative bacterium, Pseudomonas aeruginosa, in its planktonic and biofilm modes, which the latter is much more resistant to antibiotics compared to the former. <sup>69</sup> Although membrane models for P. aeruginosa have been constructed experimentally to study the physicochemical properties, <sup>120</sup>-<sup>122</sup> a membrane modeling for *P. aeruginosa* was missing. In our lab, lipid diversity of symmetric *P*. aeruginosa IM models were developed to include lipids containing a cyclopropane moiety of sn-2 tail, namely, 1-palmitoyl-2-cis-11,12-methylene-stearic-acid-sn-glycero-3-phosphoethanolamine (PMSPE) and 1-palmitoyl-2-cis-11,12-methylene-stearic-acid-sn-glycero-3-phosphoglycerol (PMSPG). The FF for the cyclopropane moiety of these lipids was adapted from the QM-based parameters for PMPE, which was developed for the IM of E. coli. 68 This was further tested against deuterium NMR data of the sn-2 chain on a single PDSPE lipid membrane.<sup>69</sup> The IM models consisted of a PE:PG ratio of 1.4 for both modes and included fatty acid chain 16:0, 16:1, 18:1, and cyC19 in 54%, 0%, 27%, and 19% for planktonic mode; in 48%, 10%, 32%, and 10% for biofilm mode. While the surface area per lipid has no significant difference in both modes, the thickness (head-to-head, bilayer, and hydrophobic) of the planktonic membrane was thicker ~1 Å than that of the biofilm membrane. The hydrophobic thicknesses of the planktonic and the biofilm membranes were  $30.4 \pm 0.1$  Å and  $29.7 \pm 0.3$  Å, respectively, in good agreement with the average hydrophobic thickness of transmembrane proteins in the P. aeruginosa IM (30.4  $\pm$  0.7 Å). The lipid relaxation time in the planktonic membrane is significantly longer than that in the biofilm membrane. The PMSPG lipid chain with a cyclopropane moiety (the sn-2 tail) has a higher order parameter at C19 but lower at C11 and C12 in the planktonic membrane, compared to the biofilm membrane. While the compression modulus has no difference in both modes, the modulus of P. aeruginosa IM is relatively smaller compared to *E coli* IM and Chlamydia trachomatis IM models.

**Outer Membrane of** *E. coli*. In previous section, our modeling efforts on lipid composition leaflet asymmetry for the bacterial IM was presented and this section focuses on the more extreme case of leaflet composition asymmetry, i.e., the outer membrane (OM) of gram-negative bacteria The OM consists of LPS with varying lengths and sugars in the outer leaflet and PL in the inner leaflet. The structure of LPS contains a glycan polymer at the outermost domain, the core oligosaccharide, and lipid A having a phosphorylated glucosamine disaccharide with multiple acyl chains. Lipid A, as the lipid anchor to the outer leaflet of the OM, is known to have varied amounts of acyl chains (4-7) and varied chain length<sup>60</sup>, depending on the bacterial species and environments. The unique asymmetric OM of gram-negative bacteria functioning as a selective barrier and resistant shell allows the bacterium to survive in many harsh environments and resist antibiotics. Most OM modeling<sup>58, 60, 102, 123, 124</sup> has been studied by a floating bilayer while the OM experimental models<sup>102, 124-127</sup> have been created as supported lipid bilayer. Our lab has modeled

homogeneous lipid A bilayers in collaboration with Wonpil Im,<sup>58, 60</sup> focusing on the topology, FF parameters, and membrane properties ( $A_{lip}$ , the hydrophobic thickness, and the chain order), and investigated 21 distinct lipid types found in bacterial species. The various neutralizing ion types ( $Ca^{2+}$ ,  $K^+$ , and  $Na^+$ ) affecting the membrane properties in terms of lipid diffusion coefficients, ion residence times, and  $K_A$ ) were also examined. The investigation revealed that the bilayer properties are mainly determined by the acyl chain number and chain length. The  $A_{lip}$  increases as a function of chain number, and the hydrophobic thickness increases as a function of chain length. An observed correlation among the  $A_{lip}$ , the hydrophobic thickness, and the chain order shown that as the order parameter increases,  $A_{lip}$  decreases, and the membrane containing a highly ordered lipid A is thicker. Also,  $Ca^{2+}$  resides longer on the head groups of lipid A, resulting in a low lateral diffusion and high compressibility of lipid A.

An E. coli OM model (LPS-PL bilayer) has also been developed for investigating the interactions between a transmembrane protein, OmpLA, and the lipid bilayer. 58 The OM consisted of Lipid A, R1 core (without O-antigen polysaccharide) for the outer leaflet and a mixture of 1-palmitoyl(16:0)-2palmitoleoyl(16:1 cis-9)-phosphatidylethanolamine (PPPE), 1-palmi-toyl(16:0)-2-vacenoyl(18:1 cis-11)phosphatidylglycerol (PVPG), and 1,10-palmitoyl-2,20-vacenoyl cardiolipin with a net charge of -2e (PVCL2) at a ratio of 15:4:1 for the inner leaflet. The structural properties of the E. coli OM showed that the hydrophobic thickness of the asymmetric LPS-PL bilayer (24. Å) is much thinner than the symmetric PL bilayer (28.3 Å) (the control) due to the thinner LPS leaflet. The hydrophobic thickness of the E. coli OM model perfectly agrees with the average hydrophobic thickness of the known outer membrane proteins (~24 Å). 128 Different lipid ratios of the asymmetric LPS-PL bilayer demonstrated no significant difference in the membrane area, density profile, and hydrophobic thickness but in changes in the chain packing, indicating the lipid self-adjusting mechanism allows the bacteria to alter the lipid ratio to keep membrane integrity. In terms of the modeling of OmpLA on membranes, the hydrophobic thickness of OmpLA is much better matched to that of the asymmetric LPS-PL bilayer than the symmetric PL bilayer. A thinning effect on the change of local membrane structure has been observed when the asymmetric bilayer facilitates OmpLA. The OmpLA loop movement analysis revealed that the reduced loop dynamics with LPS lipid led to a rigid secondary-structure formation and loop displacement, which is crucial for preventing pore formation across the barrel and keeping toxic molecules outside the OM.

The above *E. coli* OM modeling has been also applied to explore the physical properties of synthesized OM mimetics in collaboration with Göran Widmalm and Wonpil Im.<sup>102</sup> The bacterial OM model has been developed to include *E. coli K12* lipid A with the *K12* core sugars (without O-antigen) in the outer leaflet and DPPC in the inner leaflet to match the experimental model.<sup>125, 126</sup> The study connected the MD

simulation and the neutron reflectometry by converting the number density distributions profile along the bilayer normal axis (z-axis) from the OM modeling to scattering length density (SLD) which is compatible with the measurement result of neutron SLD (NSLD). Experimentally, the amount of DPPC that is in the inner vs. outer leaflet is unclear so a set of LPS-DPPC bilayers were simulated with various degrees of asymmetry ranging from 50% to 100% DPPC for the amount of DPPC in the inner leaflet. Noting that system LPS-DPPC<sup>50%</sup> represents the fully mixed symmetric bilayer system, whereas system LPS-DPPC<sup>100%</sup> represents the fully demixed system that consists of pure LPS in the outer leaflet and pure DPPC in the inner leaflet. The asymmetric membrane modeling result showed that the  $A_{lip}$  for Lipid A and DPPC and hydrophobic thickness of membrane illustrated monotonic functions in the range between 50 to 90% of the degree of asymmetry, indicating the set of bilayer modeling was a perfect scaler for identifying the degree of asymmetry of the experimental samples. Examining the synthesized floating E. coli OM model membrane, the resulting measurement using the developed scaler for SLD revealed no significant difference in lipid composition between T=293 and 310 K, indicating temperature-induced lipid translocation across leaflets on heating is unlikely in this temperature range. On the other hand, the out-of-plane fluctuations (roughness) of membrane showed as a Gaussian width of 14.7 Å at 293 K, compared to 22 Å at 310 K, as the exception for thermal driven property.

## **Yeast Membrane Models**

Membrane modeling of more complex eukaryotic organisms have also been investigated using MD simulation in our lab. Our first membrane modeling in this area was to develop a yeast-like membrane model using the early version of CHARMM-GUI *Membrane Builder*<sup>23</sup> with the CHARMM27r FF. This early model of yeast membrane composited lipids that averaged between the ER and the PM with six different lipid types (available at the time): DPPC, DOPC (1,2-dioleoyl-sn-glycero-3-phosphatidylcholine), POPE, POPA (1-palmitoyl-2-oleoyl-sn-glycero-3-phosphatic acids), and POPS (1-palmitoyl-2-oleoyl-sn-glycero-3-phosphatidylserine), and cholesterol (CHOL). This yeast-like bilayer was remarkable for being the first yeast membrane model that contained some lipid diversity compared to the earlier models with only two PLs and cholesterol. This yeast-like bilayer model was taken to further investigate the permeability of some artificial receptors. Although the simulation time was relatively short (20-30 ns) compared to what is currently used (300 ns and more), the effects of lipid tail saturation, Chol concentration, and surface tension on membrane properties were examined. The results revealed that the *A*<sub>lip</sub> increases, the order parameter decreases, and the tilt angle of Chol increases as the concentration of unsaturated chains increases.

This initial modeling was updated to develop yeast organelle membrane models for the ER, TGN, and the PM<sup>71</sup> with the more available lipid types and updated FF (C36). The models consisted of lipid head groups of PA, PC, PE, PI, PS and ergosterol (ERG) at various ratios: 5%, 12%, 13%, 12%, 18% and 40% for the PM bilayer; 4%, 47%, 13%, 23%, 3%, and 8% for the ER bilayer; 3%, 35%, 11%, 37%, 3%, and 12% for the TGN bilayer. Phospholipids of 14 lipid types containing at least one monounsaturated tail and lengths vary from 16 to 18 carbons (16:0, 16:1, 18:0, and 18:1) and ergosterol, instead of cholesterol in the previous model, have been used to construct the yeast membranes. The  $A_{lip}$  of models increased in order of PM < TGN < ER whereas the  $K_A$  of models decreased in order of PM > TGN ~ ER. The PM model demonstrated less tilt of sterols and a higher order parameter in both tails that indicates a more ordered bilayer. The PM model is thicker in hydrophobic core thickness than ER and TGN models, matching with the estimation of hydrophobic regions of transmembrane proteins from the Orientation of Proteins in Membranes database. Besides general trends of the structural, mechanical, and dynamical behavior of membranes, these yeast organelle models provided an understanding of detailed lipid information, such as fatty acid tail ordering, which has been illustrated quite differently among specific compartments in the cell from the lipid diversity modeling. The result indicated that the inclusion of lipid diversity for bilayer models better described the lipid domain of the bilayer environment, providing more accurate membranemembrane and membrane-protein interactions for cell processes.

### **Plant Membrane Models**

Moving on from single-celled organisms, we have done research on more advanced organisms such as plants. Although it is well known that the major lipids for the plant PM are sterols, sphingolipids and glycerolipids, <sup>129</sup> limited experimental data on the detailed lipid composition for plant species is available since the extraction and purification of the PM or certain lipids is challenging, <sup>130-132</sup> and there are less simulation studies of plant PM<sup>72, 133</sup> since the diversity of lipids requires a versatile lipid FF. With a wide range of lipids supported, the C36 lipid FF is now capable of modeling complex plant membranes. Soybean membrane models were constructed using a mixture of phosphatidic acid (PA), PC, PI, PE lipids and sterols and shown to be less compressible compared to the bacterial membranes. An asymmetric model for the *Arabidopsis thaliana* PM was also developed using glycerophospholipids, glycolipids and sitosterol. Glycolipids were put in the outer leaflet exclusively in this model and displayed favorable interactions with sitosterol, potentially promoting the formation of lipid rafts.

**Soybean Plasma Membrane.** Zhuang et al.<sup>72</sup> were the first to simulate a complex plant membrane model containing sterols. Membrane models based on experiments were built for the PMs (hypocotyl and root) of

soybean. The two models contain 9 and 10 different lipids including glycerophospholipids (GPLs), sitosterol and stigmasterol. The work also compared the complex model membranes to single-component linoleic acid-containing lipid membranes because linoleic-acid (18:2, cis-9,12) was present in all the GPLs of the complex models. Other acyl chains of the complex membranes are palmitic acid (16:0) and linolenic acid (18:3, cis-9,12,15). Note linoleic-acid and linolenic acid are polyunsaturated fatty acids (PUFAs) containing two or more double bonds.

The root membrane has a slightly lower  $A_{lip}$  compared to the hypocotyl due to more sterols and PA lipids with a small head group. The smaller head group of PA also allows more water penetration into the membrane so that a smaller overall thickness (D<sub>B</sub>), which measures water penetration, was observed for the root membrane. Using tilt angle and component surface area, the authors found stigmasterol is more upright in the root membrane, though the difference is small. Hydrogen bonding and lipid clustering were performed for the two model membranes, and it was found that the interaction between the sterols and GPLs is stronger than the interactions between GPLs. These analyses also indicated that the lipids of similar tail saturation prefer each other rather than the lipids with different tail saturations. The comparison with simple 1,2-dilinoleoyl-sn-glycero-3-phosphocholine (DLiPC, di-18:2, cis-9,12) lipid membrane showed a smaller component area of DLiPC in the hypocotyl membrane (62.3  $\pm$  0.4 Å<sup>2</sup> versus 70.7  $\pm$  0.2 Å<sup>2</sup>) and a corresponding larger hydrophobic thickness (32.8  $\pm$  0.2 Å versus 26.9  $\pm$  0.03 Å), which suggested a tighter packing of the hypocotyl membrane. This tight packing was more directly measured by the  $S_{CD}$  of DLiPC and was very likely caused by the ordering effect of sterol.  $K_A$  for the soybean membranes (hypocotyl: 0.51  $\pm$  0.07 N/m; root: 0.57  $\pm$  0.06 N/m) is comparable to the yeast PM and about twice the  $K_A$  of the E. coli cytoplasmic membrane, which can be explained by the sterols present in the soybean/yeast membranes but absent in the *E. coli* membrane.

Arabidopsis thaliana Plasma Membrane. Realistic PMs of eukaryotic cells are asymmetric in terms of lipid composition between leaflets like the bacterial membranes. Although simplified asymmetric membrane models have been used in simulation studies, 134-137 modeling asymmetric membrane in a more realistic manner remains challenging due to lack of experimental data. Yu and Klauda 138 recently modeled the PM of Arabidopsis Thaliana leaves based on collective experimental studies. 129, 131, 139, 140 The major lipid types detected in these experiments are GPLs, sphingolipids, and sterols. While the leaflet asymmetry was not directly determined, it is known that sphingolipids are primarily on the outer (apoplastic) leaflet due to biased lipid transportation. A simplification was made by Yu and Klauda 138 to exclude sphingolipids from the inner (cytosolic) leaflet in order to model the lipidomic asymmetry. Five different GPLs, two different sphingolipids, and one sterol (sitosterol) were used in their model. The two sphingolipids (Figure 2a), glucosylceramide (GluCer) and glycosyl inositol phosphoryl ceramide (GIPC), are characteristic

sphingolipids in plants and are also called glycolipids. Acyl chains of GPLs in the model were mostly unsaturated while the glycolipids contain more saturated tails. Two symmetric models (one for each leaflet) were built and simulated before combining them to form the asymmetric model (Figure 2b) using an areamatching method.

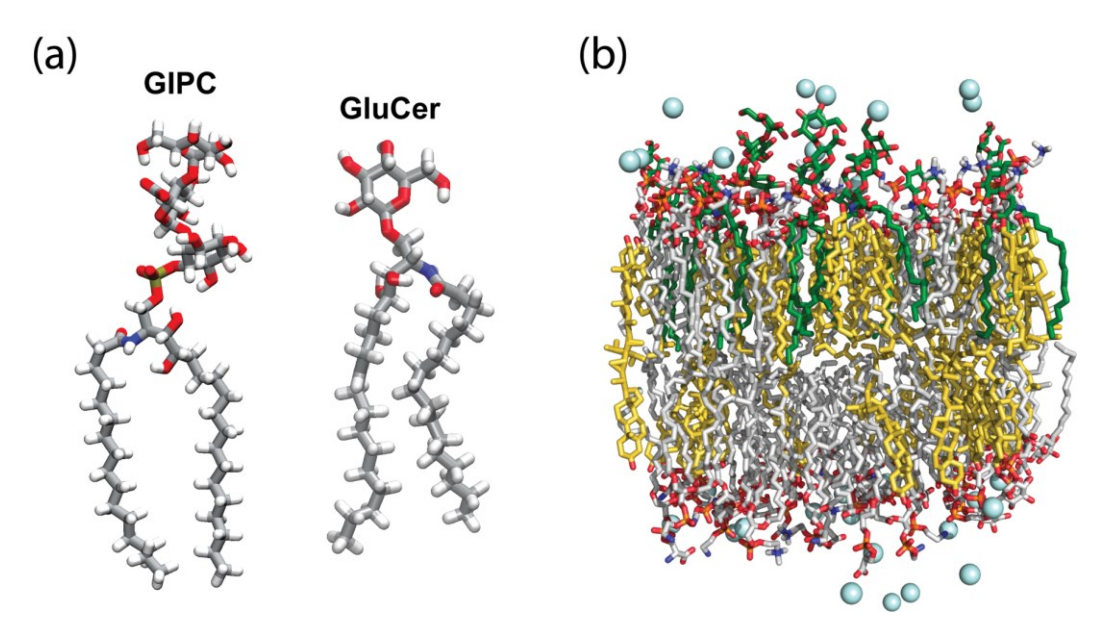


**Figure 2.** (a) Representation of a glycosyl inositol phosphoryl ceramide (GIPC) and a glycosylceramide (GluCer) from the *Arabidopsis thaliana* model membrane. Carbon in silver, oxygen in red, phosphorous in copper, nitrogen in blue. (b) The Asymmetric model for the PM of *Arabidopsis thaliana*. Carbon of GIPC and GluCer in green, carbon of sitosterol in yellow, carbon of glycerophospholipids in silver, oxygen in red, phosphorous in copper, nitrogen in blue, potassium ions shown as cyan spheres.

Analyses on these membrane models (symmetric and asymmetric) indicated that the outer leaflet is more rigid and tightly packed compared to the inner leaflet, which is consistent with the higher portions of saturated tails and sitosterol.  $K_A$  for the asymmetric membrane is  $0.94 \pm 0.04$  N/m, which is almost two times the value for the soybean membranes. Considering the fluidity of PUFAs (more in the soybean membranes) and saturated tails (more in the *Arabidopsis Thaliana* membrane), this result is expected. Pressure profiles calculated for these membranes showed overall similarity between the inner and outer leaflets. The additional huge oscillations at  $\pm 10$  Å from the center of the bilayer compared to pure GPL/sphingolipid bilayers indicated that the modification to the membrane mechanics by sitosterol is evident. It is worth noting that the spontaneous curvatures calculated for all these model membranes were negative, which suggested the importance of the interplay between lipids and membrane proteins. Clustering analysis and lipid raft analysis using hidden Markov modeling (HMM)<sup>141</sup> suggested stronger

interactions between sitosterols and glycolipids than sitosterols and GPLs. Glycolipids were found to have unfavorable interactions between each other and the bridging role of sitosterol in raft formation was hypothesized.

### **Mammalian Membrane Models**

Apart from plants, mammalian membrane models have been studied using the C36 lipid FF in our lab. Unlike plants whose major sphingolipids are glycosphingolipids, mammalian membranes contain more sphingomyelins (SMs) and ceramides (CERs). 142, 143 The lipid composition can vary wildly depending on the species and organelles, which is evident from our models for ocular lens, <sup>144</sup> stratum corneum (SC)<sup>145</sup>, <sup>146</sup> and peripheral nerve myelin. <sup>147</sup> The modeling of ocular lens focused on the influence of CHOL fraction and SM species where CHOL% ranged from 0 to 73 in the context of equal GPL/SM concentration. Two sets of models were developed for the SC, corresponding to the short periodicity phase (SPP) and the long periodicity phase (LPP). Both the SPP and LPP are repeating units based on X-ray diffraction, 143, 148 although the SPP is characterized as a simple bilayer while the LPP has a sandwich-like structure. 149 The study of the SPP covered a wide range of CER concentration and examined the effects of CER hydroxylation and free fatty acid (FFA) protonation. The sandwich model for the LPP initially proposed by the group of Bouwstra<sup>149</sup> consists of two bilayers surrounding a fluid interior slab, and further investigation suggested that CHOL is not present in the interior. 150 Our models captured these main features and replicated the compositions used by two experiments so that direct comparisons were possible. Modeling of rat peripheral nerve myelin in our group focused on the effects of CHOL concentration and PI vs. PS inspired by the dysfunction that occurs in diabetic individuals.

**Ocular Lens.** Simple ocular lens membrane models were developed by Adams et al. <sup>144</sup> An important feature of ocular lens membrane is the large portion of CHOL, which accounts up to 73% in these models. Adams et al. used two different SMs, namely dihydrosphingomyelins (DHSM) and N-nervonoyl-D-erythro-sphingosylpho-sphorylcholine (NSM), to explore the influence of the double bond at the beginning of the sphingosine chain. They also compared the complex membranes containing four lipid types (PC, PE, SM, and CHOL) to simpler mixtures with or without CHOL/PC/PE. Adding cholesterol to the system led to more compact membranes reflected by the reduced component surface area and the prominently increased  $S_{\rm CD}$  for SM/PC/PE. While most membrane properties were not significantly or directly influenced by the change from NSM to DHSM, the double bond of NSM reduced the flexibility for both the sphingosine and fatty acid chains so that deeper penetration of the NSM methyl was observed. DHSM also affected the membrane structure indirectly by altering the tilting of CHOL and the function of PE such as

hydrogen bonding with CHOL. Although the models presented in this study are simple, it provided a baseline for future simulations of more accurate ocular lens membrane models.

**Stratum Corneum Models.** *Stratum corneum*, which is the outer layer and the primary barrier of the skin, has two major components: corneocytes and the surrounding lipid matrix. <sup>151</sup> Existing simulations of the SC vary in many aspects such as lipid composition, protonation state of the FAA, number of layers, hydration, and FF. In a series of related studies, <sup>54, 145, 146, 152</sup> Wang and Klauda modeled and simulated the SPP<sup>145, 152</sup> and the LPP<sup>146</sup> with the C36 lipid FF and compared their results with experiments and simulations using other FFs. <sup>153-156</sup>

The SPP model from Wang and Klauda is a ternary mixture composed of N-lignoceroylsphingosine (CerNS)/ $\alpha$ -lignoceroylphytosphingosine (CerAP), FFA and CHOL. The effects of CER concentration, CER hydroxylation (CerNS vs. CerAP) and FFA protonation were thoroughly investigated. Among the three factors, CER concentration and hydroxylation were found to have more comprehensive influence on bilayer properties, while FFA protonation mostly induced significant changes in FFA-specific properties. For example, increasing the CER concentration induced decrease in component surface area for all the three lipids and increased  $S_{\rm CD}$  for both FFA and CER (fatty acid chain). CER hydroxylation was found to have prominent influence on hydrogen bonding. A more-than-two-fold increase in hydrogen bonds per lipid for CER was observed when hydroxylated, and the corresponding increases were 14% for CHOL and 30% for FFA. The work has also discussed the differences in the NSLD profiles between simulation and experiment. The acetate buffer used in the experiment could bind to the lipid head groups and cause widening of the head group peak around  $\pm 25$  Å. Additional peaks at  $\pm 8$  Å in the simulated profiles were potentially due to the increased disorder at the bilayer center, while in experiment the ends of the fatty acid tails protruded straight though the center and met the sphingosine chains of the opposite leaflet.

Models in bilayer-slab-bilayer (sandwich) structures for the LPP were simulated with the C36 lipid FF by Wang and Klauda, along with umbrella sampling simulations using select models (including SPP models) to study ethanol permeation through the lipid matrix. The major difference in lipid composition compared to the SPP is that 30-linoyloxytriacontanoic acid-[(2S,3R)-1,3-dihydroxyoctadec-4-enyl]-amide (CerEOS) is present in these models, which contains a long fatty acid chain (48 carbons). For each model, one monolayer with randomly selected lipids flipped to create a bidirectional slab was put at the middle and two bilayers were put at two sides to form a sandwich structure. CerEOS was only present in the outer leaflet of the bilayer and CHOL was excluded from the central slab. The study found increased CerEOS concentration can induce melting of the central slab. Different conformations for CerEOS (hooked and

extended) and CERs with shorter fatty acid chain (hairpin and extended) were observed and the time scale of transition between different conformations is typically tens of nanoseconds. Comparison with experimental density profiles indicated a thinner central slab in simulation which can be explained by the greater interdigitation among the slab lipids. The phase change of the central slab with varying CerEOS concentration was found to influence the energetics of ethanol permeation, with the central well of the PMF lowered for the disordered phase. However, the overall shapes of the PMF for different LPP models were similar and indicated a leapfrog mechanism of ethanol permeation in the LPP.

Peripheral Nerve Myelin. Myelin sheath has a multilayered structure and is a critical component of both central and peripheral nerves. Summetric fashion. Four models were built and simulated with the C36 lipid FF to investigate the influences of PI vs. PS and diabetes on membrane properties. The diabetic models contain significantly less cholesterol (13-14%) compared to the non-diabetic models (36-37%). The lowered cholesterol concentration induced a less rigid and thinner membrane measured by the lateral compressibility and a looser lipid packing which was reflected by both the component surface area and S<sub>CD</sub>. The increased fluidity of the diabetic membrane agrees with the electron spin resonance spectroscopy study by Zuvic-Butorac et al. So and corresponds well to reports of diabetic myelin sheath being more prone to damage. So the decreased cholesterol content in the diabetic membranes also induced more tilt of the sugar ring in galactosylceramide (GalCer) toward the bilayer surface due to increased inter-lipid hydrogen bonding with phospholipids, which can further deteriorate the myelin sheath in a multilayer context because of the decreased chance for GalCer to form hydrogen bonds with the opposing layers. Compared to the PI-containing membrane, PS lipids resulted in a slightly less rigid membrane, but the influence was subtle compared to the disease condition.

#### Conclusion

This *Feature Article* has reviewed our work on cell membrane modeling, involving continuous development of the C36 FF for a diversified set of lipids leading to multi-component lipid bilayer models that contain leaflet asymmetry in composition, reflecting realistic biologic membranes. For our updates to the C36 FF, we include various lipid head groups of phospholipids (PC, PE, PG, PS, PA, and PI), sphingolipids, ceramides, glycolipids, lipopolysaccharides, and lipid fatty acid chains (polyunsaturated, branched, and cyclic-containing), using the QM-based parameters and verified by available experimental data for structural and mechanical properties. These efforts remove the limitation of parameterized lipids

and lead to developing species-specific lipid bilayers for general availability in the field. Several realistic membrane models of bacteria (gram-negative bacterial outer membranes and cytoplasmic membranes), single-celled organism (yeast organelle membranes), plant (PM of soybean and *Arabidopsis thaliana*), and mammalian (ocular lens, *stratum corneum*, and peripheral nerve myelin) have been developed focusing on comprehensive diversity in lipid head group and fatty acid chains and initial leaflet asymmetry in composition recently in our lab. These models better reflect the structural and mechanical properties of membranes composed of varied compositions when compared to available experimental data. They also demonstrate the capability of lipid diversity and leaflet asymmetry in modeling lipid bilayer for many species and provide the detailed molecular information for natural and engineered cellular bilayers.

Our recently updated C36/LJ-PME improves the accuracy of the FF by adding the long-range dispersion and eliminates the FF's dependence on the LJ cutoff, which are particularly beneficial for heterogeneous lipid bilayers and monolayers while imposing minimal effects on systems insensitive to the cutoff (i.e., proteins). This updated FF demonstrates good agreement in lipid packing and relaxation time at various carbon positions and will prompt accurate simulations of protein or other macromolecules interacting with monolayers and bilayers. On the other hand, biomembrane models focusing on leaflet asymmetry in lipid composition have been constructed and simulated for the *E. coli* IM (without sterol) and *Arabidopsis thaliana* PM (with sterol) which vary in composition between the inner and outer leaflets. A more extreme case for leaflet asymmetry, the *E. coli* OM, has also been modeled. This leaflet asymmetry in composition can lead to variations of leaflet properties as observed in the asymmetric *E. coli* IM and *Arabidopsis thaliana* PM. Moreover, modeling leaflet asymmetry improves the ability to describe the natural bilayer and how lipid composition and asymmetry influences biological processes. For example, TM proteins orient in the membrane by the positive inside rule to match with the more negative-charged lipids that exist at the inner leaflet.

Accurate and diverse FFs for lipids allow for more realistic bilayers reflecting a native-like setting for complex biological processes and provide estimates for the structural, mechanical, and dynamic properties of the modelled cellular membrane. The current field is now at a state that we can begin to develop accurate model membranes of organelles in simple to complex organisms. Ultimately, it will be important to simulate larger membranes in longer timescales with proteins, nucleic acids, and carbohydrates using all-atom FFs and the next-generation polarizable FFs that future developments in improving computing power will enable. This future work will help us understand the heterogeneity and dynamics of realistic membranes and the elaborate interplays between these macromolecules leading toward potentially models that represent whole organelles and even cells.

## Acknowledgements

This research was supported in part by three NSF grants (MCB-1951425, CHE-2003912, and CHE-2029900) and the Intramural Research Program of the NIH (National Heart, Lung, and Blood Institute, NHLBI).

### References

- 1. van Meer, G.; Voelker, D. R.; Feigenson, G. W., Membrane lipids: where they are and how they behave. *Nature Reviews Molecular Cell Biology* **2008**, *9* (2), 112-124.
- 2. Worzfeld, T.; Offermanns, S., Semaphorins and plexins as therapeutic targets. *Nat. Rev. Drug Discov.* **2014**, *13* (8), 603-621.
- 3. Hong, C. Y.; Han, C.-T.; Chao, L., Nonspecific Binding Domains in Lipid Membranes Induced by Phospholipase A2. *Langmuir* **2016**, *32* (27), 6991-6999.
- 4. Gahan, C. G.; Patel, S. J.; Chen, L. M.; Manson, D. E.; Ehmer, Z. J.; Blackwell, H. E.; Van Lehn, R. C.; Lynn, D. M., Bacterial Quorum Sensing Signals Promote Large-Scale Remodeling of Lipid Membranes. *Langmuir* **2021**, *37* (30), 9120-9136.
- 5. Joseph, D.; Pidathala, S.; Mallela, A. K.; Penmatsa, A., Structure and Gating Dynamics of Na+/CI- Coupled Neurotransmitter Transporters. *Front. Mol. Biosci.* **2019**, *6*, 16.
- 6. Forrest, L. R.; Kramer, R.; Ziegler, C., The structural basis of secondary active transport mechanisms. *Biochim. Biophys. Acta-Bioenerg.* **2011**, *1807* (2), 167-188.
- 7. Zgurskaya, H. I., Introduction: Transporters, Porins, and Efflux Pumps. *Chem. Rev.* **2021**, *121* (9), 5095-5097.
- 8. Sakai-Kato, K.; Yoshida, K.; Takechi-Haraya, Y.; Izutsu, K.-i., Physicochemical Characterization of Liposomes That Mimic the Lipid Composition of Exosomes for Effective Intracellular Trafficking. *Langmuir* **2020**, *36* (42), 12735-12744.
- 9. Du, X.; Brown, A. J.; Yang, H., Novel mechanisms of intracellular cholesterol transport: oxysterol-binding proteins and membrane contact sites. *Curr Opin Cell Biol* **2015**, *35*, 37-42.
- 10. Phillips, M. J.; Voeltz, G. K., Structure and function of ER membrane contact sites with other organelles. *Nat Rev Mol Cell Biol* **2016**, *17* (2), 69-82.
- 11. Tong, J.; Manik, M. K.; Im, Y. J., Structural basis of sterol recognition and nonvesicular transport by lipid transfer proteins anchored at membrane contact sites. *Proc. Natl. Acad. Sci. U.S.A.* **2018,** *115* (5), E856-E865.
- 12. Michaud, M.; Jouhet, J., Lipid Trafficking at Membrane Contact Sites During Plant Development and Stress Response. *Front Plant Sci* **2019**, *10*, 2.

- 13. Shukla, S.; Baumgart, T., Enzymatic trans-bilayer lipid transport: Mechanisms, efficiencies, slippage, and membrane curvature. *Biochim. Biophys. Acta-Biomembr.* **2021**, *1863* (3), 13.
- 14. Johnston, L. J., Nanoscale Imaging of Domains in Supported Lipid Membranes. *Langmuir* **2007**, 23 (11), 5886-5895.
- 15. McConnell, H. M.; De Koker, R., Equilibrium Thermodynamics of Lipid Monolayer Domains. *Langmuir* **1996**, *12* (20), 4897-4904.
- 16. Schneider, R.; Brugger, B.; Sandhoff, R.; Zellnig, G.; Leber, A.; Lampl, M.; Athenstaedt, K.; Hrastnik, C.; Eder, S.; Duam, G.; Paltauf, F.; Wieland, F. T.; Kohlwein, S. D., Electrospray Ionization Tandem Mass Spectrometry (ESI-MS/MS) Analysis of the Lipid Molecular Species Composition of Yeast Subcellular Membranes Reveals Acyl Chain-based Sorting/Remodeling of Distinct Molecular Species En Route to the Plasma Membrane. *The Journal of Cell Biology* **1999**, *146* (4), 741-754.
- 17. Tuller, G.; Nemec, T.; Hrastnik, C.; Daum, G., Lipid composition of subcellular membranes of an FY1679-derived haploid yeast wild-type strain grown on different carbon sources. *Yeast* **1999**, *15* (14), 1555-1564.
- 18. Kamp, J. A. F. O. d., Lipid Asymmetry in Membranes. *Annual Review of Biochemistry* **1979**, *48* (1), 47-71.
- 19. Verkleij, A. J.; Zwaal, R. F.; Roelofsen, B.; Comfurius, P.; Kastelijn, D.; van Deenen, L. L., The asymmetric distribution of phospholipids in the human red cell membrane. A combined study using phospholipases and freeze-etch electron microscopy. *Biochimica et biophysica acta* **1973**, *323* (2), 178-93.
- 20. Lorent, J. H.; Levental, K. R.; Ganesan, L.; Rivera-Longsworth, G.; Sezgin, E.; Doktorova, M.; Lyman, E.; Levental, I., Plasma membranes are asymmetric in lipid unsaturation, packing and protein shape. *Nature Chemical Biology* **2020**, *16* (6), 644-652.
- 21. Dazzoni, R.; Buré, C.; Morvan, E.; Grélard, A.; Gounou, C.; Schmitter, J.-M.; Loquet, A.; Larijani, B.; Dufourc, E. J., Tandem NMR and Mass Spectrometry Analysis of Human Nuclear Membrane Lipids. *Analytical Chemistry* **2020**, *92* (10), 6858-6868.
- 22. Segall, S. D.; Artz, W. E.; Raslan, D. S.; Jham, G. N.; Takahashi, J. A., Triacylglycerol Composition of Coffee Beans (Coffea canephora P.) by Reversed Phase High-Performance Liquid Chromatography and Positive Electrospray Tandem Mass Spectroscopy. *Journal of Agricultural and Food Chemistry* **2005**, *53* (25), 9650-9655.
- 23. Jo, S.; Lim, J. B.; Klauda, J. B.; Im, W., CHARMM-GUI Membrane Builder for Mixed Bilayers and Its Application to Yeast Membranes. *Biophysical Journal* **2009**, *97* (1), 50-58.
- 24. Jo, S.; Kim, T.; Im, W., Automated builder and database of protein/membrane complexes for molecular dynamics simulations. *PLoS One* **2007**, *2* (9), e880-e880.

- 25. Jo, S.; Kim, T.; Iyer, V. G.; Im, W., CHARMM-GUI: a web-based graphical user interface for CHARMM. *J Comput Chem* **2008**, *29* (11), 1859-65.
- 26. Wu, E. L.; Cheng, X.; Jo, S.; Rui, H.; Song, K. C.; Dávila-Contreras, E. M.; Qi, Y.; Lee, J.; Monje-Galvan, V.; Venable, R. M.; Klauda, J. B.; Im, W., CHARMM-GUI Membrane Builder toward realistic biological membrane simulations. *J Comput Chem* **2014**, *35* (27), 1997-2004.
- 27. Wassenaar, T. A.; Ingólfsson, H. I.; Böckmann, R. A.; Tieleman, D. P.; Marrink, S. J., Computational Lipidomics with insane: A Versatile Tool for Generating Custom Membranes for Molecular Simulations. *Journal of Chemical Theory and Computation* **2015**, *11* (5), 2144-2155.
- 28. Leonard, A. N.; Wang, E.; Monje-Galvan, V.; Klauda, J. B., Developing and Testing of Lipid Force Fields with Applications to Modeling Cellular Membranes. *Chem. Rev.* **2019**, *119* (9), 6227-6269.
- 29. Klauda, J. B., Perspective: Computational modeling of accurate cellular membranes with molecular resolution. *The Journal of Chemical Physics* **2018**, *149* (22), 220901.
- 30. Marrink, S. J.; Corradi, V.; Souza, P. C. T.; Ingólfsson, H. I.; Tieleman, D. P.; Sansom, M. S. P., Computational Modeling of Realistic Cell Membranes. *Chem. Rev.* **2019**, *119* (9), 6184-6226.
- 31. Javanainen, M.; Lamberg, A.; Cwiklik, L.; Vattulainen, I.; Ollila, O. H. S., Atomistic Model for Nearly Quantitative Simulations of Langmuir Monolayers. *Langmuir* **2018**, *34* (7), 2565-2572.
- 32. Dickson, C. J.; Madej, B. D.; Skjevik, Å. A.; Betz, R. M.; Teigen, K.; Gould, I. R.; Walker, R. C., Lipid14: The Amber Lipid Force Field. *Journal of Chemical Theory and Computation* **2014**, *10* (2), 865-879.
- 33. Jämbeck, J. P. M.; Lyubartsev, A. P., An Extension and Further Validation of an All-Atomistic Force Field for Biological Membranes. *Journal of Chemical Theory and Computation* **2012**, *8* (8), 2938-2948.
- 34. Jämbeck, J. P. M.; Lyubartsev, A. P., Another Piece of the Membrane Puzzle: Extending Slipids Further. *Journal of Chemical Theory and Computation* **2013**, *9* (1), 774-784.
- 35. Dickson, C. J.; Rosso, L.; Betz, R. M.; Walker, R. C.; Gould, I. R., GAFFlipid: a General Amber Force Field for the accurate molecular dynamics simulation of phospholipid. *Soft Matter* **2012**, *8* (37), 9617-9627.
- 36. Maciejewski, A.; Pasenkiewicz-Gierula, M.; Cramariuc, O.; Vattulainen, I.; Rog, T., Refined OPLS All-Atom Force Field for Saturated Phosphatidylcholine Bilayers at Full Hydration. *The Journal of Physical Chemistry B* **2014**, *118* (17), 4571-4581.
- 37. Klauda, J. B.; Venable, R. M.; Freites, J. A.; O'Connor, J. W.; Tobias, D. J.; Mondragon-Ramirez, C.; Vorobyov, I.; MacKerell, A. D.; Pastor, R. W., Update of the CHARMM All-Atom Additive Force Field for Lipids: Validation on Six Lipid Types. *Journal of Physical Chemistry B* **2010**, *114* (23), 7830-7843.

- 38. Ponder, J. W.; Wu, C.; Ren, P.; Pande, V. S.; Chodera, J. D.; Schnieders, M. J.; Haque, I.; Mobley, D. L.; Lambrecht, D. S.; DiStasio, R. A.; Head-Gordon, M.; Clark, G. N. I.; Johnson, M. E.; Head-Gordon, T., Current Status of the AMOEBA Polarizable Force Field. *The Journal of Physical Chemistry B* **2010**, *114* (8), 2549-2564.
- 39. Chowdhary, J.; Harder, E.; Lopes, P. E. M.; Huang, L.; MacKerell, A. D.; Roux, B., A Polarizable Force Field of Dipalmitoylphosphatidylcholine Based on the Classical Drude Model for Molecular Dynamics Simulations of Lipids. *The Journal of Physical Chemistry B* **2013**, *117* (31), 9142-9160.
- 40. Li, H.; Chowdhary, J.; Huang, L.; He, X.; MacKerell, A. D.; Roux, B., Drude Polarizable Force Field for Molecular Dynamics Simulations of Saturated and Unsaturated Zwitterionic Lipids. *Journal of Chemical Theory and Computation* **2017**, *13* (9), 4535-4552.
- 41. Lee, S.; Tran, A.; Allsopp, M.; Lim, J. B.; Hénin, J.; Klauda, J. B., CHARMM36 United Atom Chain Model for Lipids and Surfactants. *The Journal of Physical Chemistry B* **2014**, *118* (2), 547-556.
- 42. Yu, Y.; Klauda, J. B., Update of the CHARMM36 United Atom Chain Model for Hydrocarbons and Phospholipids. *Journal of Physical Chemistry B* **2020**, *124* (31), 6797-6812.
- 43. Berger, O.; Edholm, O.; Jähnig, F., Molecular dynamics simulations of a fluid bilayer of dipalmitoylphosphatidylcholine at full hydration, constant pressure, and constant temperature. *Biophysical Journal* **1997**, *72* (5), 2002-2013.
- 44. Chiu, S. W.; Clark, M. M.; Jakobsson, E.; Subramaniam, S.; Scott, H. L., Optimization of Hydrocarbon Chain Interaction Parameters: Application to the Simulation of Fluid Phase Lipid Bilayers. *The Journal of Physical Chemistry B* **1999**, *103* (30), 6323-6327.
- 45. Kukol, A., Lipid Models for United-Atom Molecular Dynamics Simulations of Proteins. *Journal of Chemical Theory and Computation* **2009**, *5* (3), 615-626.
- 46. Marrink, S. J.; de Vries, A. H.; Mark, A. E., Coarse Grained Model for Semiquantitative Lipid Simulations. *The Journal of Physical Chemistry B* **2004**, *108* (2), 750-760.
- 47. Arnarez, C.; Uusitalo, J. J.; Masman, M. F.; Ingólfsson, H. I.; de Jong, D. H.; Melo, M. N.; Periole, X.; de Vries, A. H.; Marrink, S. J., Dry Martini, a Coarse-Grained Force Field for Lipid Membrane Simulations with Implicit Solvent. *Journal of Chemical Theory and Computation* **2015**, *11* (1), 260-275.
- 48. Jämbeck, J. P. M.; Lyubartsev, A. P., Derivation and Systematic Validation of a Refined All-Atom Force Field for Phosphatidylcholine Lipids. *The Journal of Physical Chemistry B* **2012**, *116* (10), 3164-3179.
- 49. Chiu, S.-W.; A. Pandit, S.; L. Scott, H.; Jakobsson, E., An Improved United Atom Force Field for Simulation of Mixed Lipid Bilayers. *The Journal of Physical Chemistry B* **2009**, *113* (9), 2748-2763.

- 50. Essmann, U.; Perera, L.; Berkowitz, M. L.; Darden, T.; Lee, H.; Pedersen, L. G., A smooth particle mesh Ewald method. *The Journal of Chemical Physics* **1995**, *103* (19), 8577-8593.
- 51. Zhuang, X.; Dávila-Contreras, E. M.; Beaven, A. H.; Im, W.; Klauda, J. B., An extensive simulation study of lipid bilayer properties with different head groups, acyl chain lengths, and chain saturations. *Biochimica et Biophysica Acta (BBA) Biomembranes* **2016**, *1858* (12), 3093-3104.
- 52. Wu, E. L.; Qi, Y.; Song, K. C.; Klauda, J. B.; Im, W., Preferred Orientations of Phosphoinositides in Bilayers and Their Implications in Protein Recognition Mechanisms. *The Journal of Physical Chemistry B* **2014**, *118* (16), 4315-4325.
- Venable, Richard M.; Sodt, Alexander J.; Rogaski, B.; Rui, H.; Hatcher, E.; MacKerell, Alexander D., Jr.; Pastor, Richard W.; Klauda, Jeffery B., CHARMM All-Atom Additive Force Field for Sphingomyelin: Elucidation of Hydrogen Bonding and of Positive Curvature. *Biophysical Journal* **2014**, *107* (1), 134-145.
- 54. Wang, E.; Klauda, J. B., Molecular Dynamics Simulations of Ceramide and Ceramide-Phosphatidylcholine Bilayers. *The Journal of Physical Chemistry B* **2017**, *121* (43), 10091-10104.
- Wang, E.; Klauda, J. B., Examination of Mixtures Containing Sphingomyelin and Cholesterol by Molecular Dynamics Simulations. *The Journal of Physical Chemistry B* **2017**, *121* (18), 4833-4844.
- 56. Leonard, A. N.; Pastor, R. W.; Klauda, J. B., Parameterization of the CHARMM All-Atom Force Field for Ether Lipids and Model Linear Ethers. *Journal of Physical Chemistry B* **2018**, *122* (26), 6744-6754.
- 57. West, A.; Zoni, V.; Teague, W. E.; Leonard, A. N.; Vanni, S.; Gawrisch, K.; Tristram-Nagle, S.; Sachs, J. N.; Klauda, J. B., How Do Ethanolamine Plasmalogens Contribute to Order and Structure of Neurological Membranes? *The Journal of Physical Chemistry B* **2020**, *124* (5), 828-839.
- 58. Wu, Emilia L.; Fleming, Patrick J.; Yeom, Min S.; Widmalm, G.; Klauda, Jeffery B.; Fleming, Karen G.; Im, W., E. coli Outer Membrane and Interactions with OmpLA. *Biophysical Journal* **2014**, *106* (11), 2493-2502.
- 59. Jo, S.; Wu, E. L.; Stuhlsatz, D.; Klauda, J. B.; MacKerell, A. D.; Widmalm, G.; Im, W., Lipopolysaccharide Membrane Building and Simulation. In *Glycoinformatics*, Lütteke, T.; Frank, M., Eds. Springer New York: New York, NY, 2015; pp 391-406.
- 60. Kim, S.; Patel, Dhilon S.; Park, S.; Slusky, J.; Klauda, Jeffery B.; Widmalm, G.; Im, W., Bilayer Properties of Lipid A from Various Gram-Negative Bacteria. *Biophysical Journal* **2016**, *111* (8), 1750-1760.
- 61. Patel, Dhilon S.; Park, S.; Wu, Emilia L.; Yeom, Min S.; Widmalm, G.; Klauda, Jeffery B.; Im, W., Influence of Ganglioside GM1 Concentration on Lipid Clustering and Membrane Properties and Curvature. *Biophysical Journal* **2016**, *111* (9), 1987-1999.

- 62. Guvench, O.; S. Mallajosyula, S.; Prabhu Raman, E.; Hatcher, E.; Vanommeslaeghe, K.; J. Foster, T.; W. Jamison, F.; D. MacKerell, A., CHARMM Additive All-Atom Force Field for Carbohydrate Derivatives and Its Utility in Polysaccharide and Carbohydrate–Protein Modeling. *Journal of Chemical Theory and Computation* **2011**, *7* (10), 3162-3180.
- 63. Mallajosyula, S. S.; Guvench, O.; Hatcher, E.; MacKerell, A. D., CHARMM Additive All-Atom Force Field for Phosphate and Sulfate Linked to Carbohydrates. *Journal of Chemical Theory and Computation* **2012**, *8* (2), 759-776.
- 64. Raman, E. P.; Guvench, O.; MacKerell, A. D., CHARMM Additive All-Atom Force Field for Glycosidic Linkages in Carbohydrates Involving Furanoses. *The Journal of Physical Chemistry B* **2010**, *114* (40), 12981-12994.
- 65. Guvench, O.; Hatcher, E.; Venable, R. M.; Pastor, R. W.; MacKerell, A. D., CHARMM Additive All-Atom Force Field for Glycosidic Linkages between Hexopyranoses. *Journal of Chemical Theory and Computation* **2009**, *5* (9), 2353-2370.
- 66. Klauda, J. B.; Monje, V.; Kim, T.; Im, W., Improving the CHARMM force field for polyunsaturated fatty acid chains. *Journal of Physical Chemistry B* **2012**, *116* (31), 9424-9431.
- 67. Lim, J. B.; Klauda, J. B., Branching at the Iso- and Anteiso- Positions in Complex Chlamydia Membranes: A Molecular Dynamics Study. *Biochimica et Biophysica Acta (BBA) Biomembranes* **2011**, *1808* (1), 323-331
- 68. Pandit, K. R.; Klauda, J. B., Membrane models of *E. coli* containing cyclic moieties in the aliphatic lipid chain. *Biochimica et Biophysica Acta (BBA) Biomembranes* **2012**, *1818* (5), 1205-1210.
- 69. Yu, Y.; Klauda, J. B., Modeling Pseudomonas aeruginosa inner plasma membrane in planktonic and biofilm modes. *The Journal of Chemical Physics* **2018**, *149* (21), 215102.
- 70. Lim, J. B.; Rogaski, B.; Klauda, J. B., Update of the Cholesterol Force Field Parameters in CHARMM. *The Journal of Physical Chemistry B* **2012**, *116* (1), 203-210.
- 71. Monje-Galvan, V.; Klauda, J. B., Modelling Yeast Organelle Membranes and How Lipid Diversity influences Bilayer Properties. *Biochemistry* **2015**, *54* (45), 6852-6861.
- 72. Zhuang, X.; Ou, A.; Klauda, J. B., Simulations of simple linoleic acid-containing lipid membranes and models for the soybean plasma membranes. *The Journal of Chemical Physics* **2017**, *146* (21), 215103.
- 73. Xu, Y.; Huang, J., Validating the CHARMM36m protein force field with LJ-PME reveals altered hydrogen bonding dynamics under elevated pressures. *Communications Chemistry* **2021**, *4* (1), 99.
- 74. Leonard, A. N.; Simmonett, A. C.; Pickard, F. C.; Huang, J.; Venable, R. M.; Klauda, J. B.; Brooks, B. R.; Pastor, R. W., Comparison of Additive and Polarizable Models with Explicit Treatment of

- Long-Range Lennard-Jones Interactions Using Alkane Simulations. *Journal of Chemical Theory and Computation* **2018**, *14* (2), 948-958.
- 75. Klauda, J. B.; Wu, X.; Pastor, R. W.; Brooks, B. R., Long-Range Lennard-Jones and Electrostatic Interactions in Interfaces: Application of the Isotropic Periodic Sum Method. *The Journal of Physical Chemistry B* **2007**, *111* (17), 4393-4400.
- 76. Mecke, M.; Winkelmann, J.; Fischer, J., Molecular Dynamics Simulation of the Liquid-Vapor Interface: The Lennard-Jones Fluid. *Journal of Chemical Physics* **1997**, *107*, 9264-9270.
- 77. Yu, Y.; Krämer, A.; Venable, R. M.; Simmonett, A. C.; MacKerell, A. D.; Klauda, J. B.; Pastor, R. W.; Brooks, B. R., Semi-automated Optimization of the CHARMM36 Lipid Force Field to Include Explicit Treatment of Long-Range Dispersion. *Journal of Chemical Theory and Computation* **2021**, *17* (3), 1562-1580.
- 78. Yu, Y.; Krämer, A.; Venable, R. M.; Brooks, B. R.; Klauda, J. B.; Pastor, R. W., CHARMM36 Lipid Force Field with Explicit Treatment of Long-Range Dispersion: Parametrization and Validation for Phosphatidylethanolamine, Phosphatidylglycerol, and Ether Lipids. *Journal of Chemical Theory and Computation* **2021**, *17* (3), 1581-1595.
- 79. Lagüe, P.; Pastor, R. W.; Brooks, B. R., Pressure-Based Long-Range Correction for Lennard-Jones Interactions in Molecular Dynamics Simulations: Application to Alkanes and Interfaces. *The Journal of Physical Chemistry B* **2004**, *108* (1), 363-368.
- 80. Klauda, J. B., Considerations of Recent All-Atom Lipid Force Field Development. *The Journal of Physical Chemistry B* **2021**, *125* (22), 5676-5682.
- 81. Durell, S. R.; Brooks, B. R.; Ben-Naim, A., Solvent-Induced Forces between Two Hydrophilic Groups. *Journal of Physical Chemistry* **1994**, *98* (8), 2198-2202.
- 82. Jorgensen, W. L.; Chandrasekhar, J.; Madura, J. D.; Impey, R. W.; Klein, M. L., Comparison of simple potential functions for simulating liquid water. *The Journal of Chemical Physics* **1983**, *79* (2), 926-935.
- 83. Wennberg, C. L.; Murtola, T.; Páll, S.; Abraham, M. J.; Hess, B.; Lindahl, E., Direct-Space Corrections Enable Fast and Accurate Lorentz-Berthelot Combination Rule Lennard-Jones Lattice Summation. *Journal of Chemical Theory and Computation* **2015**, *11* (12), 5737-5746.
- 84. Abraham, M. J.; Murtola, T.; Schulz, R.; Páll, S.; Smith, J. C.; Hess, B.; Lindahl, E., GROMACS: High performance molecular simulations through multi-level parallelism from laptops to supercomputers. *SoftwareX* **2015**, *1-2*, 19-25.
- 85. Brooks, B. R.; Brooks, C. L.; Mackerell, A. D.; Nilsson, L.; Petrella, R. J.; Roux, B.; Won, Y.; Archontis, G.; Bartels, C.; Boresch, S.; Caflisch, A.; Caves, L.; Cui, Q.; Dinner, A. R.; Feig, M.; Fischer, S.; Gao, J.; Hodoscek, M.; Im, W.; Kuczera, K.; Lazaridis, T.; Ma, J.; Ovchinnikov, V.;

- Paci, E.; Pastor, R. W.; Post, C. B.; Pu, J. Z.; Schaefer, M.; Tidor, B.; Venable, R. M.; Woodcock, H. L.; Wu, X.; Yang, W.; York, D. M.; Karplus, M., CHARMM: The biomolecular simulation program. *Journal of Computational Chemistry* **2009**, *30* (10), 1545-1614.
- 86. Eastman, P.; Swails, J.; Chodera, J. D.; McGibbon, R. T.; Zhao, Y.; Beauchamp, K. A.; Wang, L.-P.; Simmonett, A. C.; Harrigan, M. P.; Stern, C. D.; Wiewiora, R. P.; Brooks, B. R.; Pande, V. S., OpenMM 7: Rapid development of high performance algorithms for molecular dynamics. *PLOS Computational Biology* **2017**, *13* (7), e1005659.
- 87. Hong, C.; Tieleman, D. P.; Wang, Y., Microsecond Molecular Dynamics Simulations of Lipid Mixing. *Langmuir* **2014**, *30* (40), 11993-12001.
- 88. Murzyn, K.; Róg, T.; Pasenkiewicz-Gierula, M., Phosphatidylethanolamine-phosphatidylglycerol bilayer as a model of the inner bacterial membrane. *Biophys J* **2005**, *88* (2), 1091-103.
- 89. Zhao, W.; Róg, T.; Gurtovenko, A. A.; Vattulainen, I.; Karttunen, M., Role of phosphatidylglycerols in the stability of bacterial membranes. *Biochimie* **2008**, *90* (6), 930-8.
- 90. Soliman, W.; Bhattacharjee, S.; Kaur, K., Interaction of an Antimicrobial Peptide with a Model Lipid Bilayer Using Molecular Dynamics Simulation. *Langmuir* **2009**, *25* (12), 6591-6595.
- 91. Lee, J.; Jung, S. W.; Cho, A. E., Molecular Insights into the Adsorption Mechanism of Human β-Defensin-3 on Bacterial Membranes. *Langmuir* **2016**, *32* (7), 1782-1790.
- 92. Kostritskii, A. Y.; Kondinskaia, D. A.; Nesterenko, A. M.; Gurtovenko, A. A., Adsorption of Synthetic Cationic Polymers on Model Phospholipid Membranes: Insight from Atomic-Scale Molecular Dynamics Simulations. *Langmuir* **2016**, *32* (40), 10402-10414.
- 93. Zhang, Y.; Chen, T.; Pan, Z.; Sun, X.; Yin, X.; He, M.; Xiao, S.; Liang, H., Theoretical Insights into the Interactions between Star-Shaped Antimicrobial Polypeptides and Bacterial Membranes. *Langmuir* **2018**, *34* (44), 13438-13448.
- 94. Paul, R.; Paul, S., Translocation of Endo-Functionalized Molecular Tubes across Different Lipid Bilayers: Atomistic Molecular Dynamics Simulation Study. *Langmuir* **2021**, *37* (34), 10376-10387.
- 95. Silva, T.; Claro, B.; Silva, B. F. B.; Vale, N.; Gomes, P.; Gomes, M. S.; Funari, S. S.; Teixeira, J.; Uhríková, D.; Bastos, M., Unravelling a Mechanism of Action for a Cecropin A-Melittin Hybrid Antimicrobial Peptide: The Induced Formation of Multilamellar Lipid Stacks. *Langmuir* **2018**, *34* (5), 2158-2170.
- 96. Sanders, M. R.; Clifton, L. A.; Frazier, R. A.; Green, R. J., Role of Lipid Composition on the Interaction between a Tryptophan-Rich Protein and Model Bacterial Membranes. *Langmuir* **2016**, *32* (8), 2050-2057.

- 97. Luchini, A.; Cavasso, D.; Radulescu, A.; D'Errico, G.; Paduano, L.; Vitiello, G., Structural Organization of Cardiolipin-Containing Vesicles as Models of the Bacterial Cytoplasmic Membrane. *Langmuir* **2021**, *37* (28), 8508-8516.
- 98. Tsukamoto, M.; Zappala, E.; Caputo, G. A.; Kikuchi, J.-i.; Najarian, K.; Kuroda, K.; Yasuhara, K., Mechanistic Study of Membrane Disruption by Antimicrobial Methacrylate Random Copolymers by the Single Giant Vesicle Method. *Langmuir* **2021**, *37* (33) 9982-9995.
- 99. Phambu, N.; Almarwani, B.; Alwadai, A.; Phambu, E. N.; Faciane, N.; Marion, C.; Sunda-Meya, A., Calorimetric and Spectroscopic Studies of the Effects of the Cell Penetrating Peptide Pep-1 and the Antimicrobial Peptide Combi-2 on Vesicles Mimicking Escherichia coli Membrane. *Langmuir* **2017**, *33* (45), 12908-12915.
- 100. Xing, X.; Ma, W.; Zhao, X.; Wang, J.; Yao, L.; Jiang, X.; Wu, Z., Interaction between Surface Charge-Modified Gold Nanoparticles and Phospholipid Membranes. *Langmuir* **2018**, *34* (42), 12583-12589.
- 101. Khakbaz, P.; Klauda, J. B., Probing the importance of lipid diversity in cell membranes via molecular simulation. *Chemistry and Physics of Lipids* **2015**, *192*, 12-22.
- 102. Hughes, A. V.; Patel, D. S.; Widmalm, G.; Klauda, J. B.; Clifton, L. A.; Im, W., Physical Properties of Bacterial Outer Membrane Models: Neutron Reflectometry & Molecular Simulation. *Biophysical Journal* **2019**, *116* (6), 1095-1104.
- 103. Hsieh, M.-K.; Klauda, J. B., Leaflet Asymmetry Modeling in Lipid Composition of Escherichia coli Cytoplasmic Membrane. *Journal of Physical Chemistry B* **2021**, *Submitted*.
- 104. Matsuzaki, K.; Sugishita, K.; Harada, M.; Fujii, N.; Miyajima, K., Interactions of an antimicrobial peptide, magainin 2, with outer and inner membranes of Gram-negative bacteria. *Biochimica et biophysica acta* **1997**, *1327* (1), 119-30.
- 105. Lohner, K.; Prenner, E. J., Differential scanning calorimetry and X-ray diffraction studies of the specificity of the interaction of antimicrobial peptides with membrane-mimetic systems. *Biochimica et biophysica acta* **1999**, *1462* (1-2), 141-56.
- 106. Oursel, D.; Loutelier-Bourhis, C.; Orange, N.; Chevalier, S.; Norris, V.; Lange, C. M., Lipid composition of membranes of Escherichia coli by liquid chromatography/tandem mass spectrometry using negative electrospray ionization. *Rapid Commun Mass Spectrom* **2007**, *21* (11), 1721-8.
- 107. Gidden, J.; Denson, J.; Liyanage, R.; Ivey, D. M.; Lay, J. O., Lipid Compositions in Escherichia coli and Bacillus subtilis During Growth as Determined by MALDI-TOF and TOF/TOF Mass Spectrometry. *Int J Mass Spectrom* **2009**, *283* (1-3), 178-184.
- 108. Unsay, J. D.; Cosentino, K.; Subburaj, Y.; García-Sáez, A. J., Cardiolipin Effects on Membrane Structure and Dynamics. *Langmuir* **2013**, *29* (51), 15878-15887.

- 109. Boyd, K. J.; Alder, N. N.; May, E. R., Buckling Under Pressure: Curvature-Based Lipid Segregation and Stability Modulation in Cardiolipin-Containing Bilayers. *Langmuir* **2017**, *33* (27), 6937-6946.
- 110. Tan, Z.; Khakbaz, P.; Chen, Y.; Lombardo, J.; Yoon, J. M.; Shanks, J. V.; Klauda, J. B.; Jarboe, L. R., Engineering Escherichia coli membrane phospholipid head distribution improves tolerance and production of biorenewables. *Metabolic Engineering* **2017**, *44*, 1-12.
- 111. Heijne, G., The distribution of positively charged residues in bacterial inner membrane proteins correlates with the trans-membrane topology. *EMBO J* **1986**, *5* (11), 3021-3027.
- 112. Crane, J. M.; Kiessling, V.; Tamm, L. K., Measuring Lipid Asymmetry in Planar Supported Bilayers by Fluorescence Interference Contrast Microscopy. *Langmuir* **2005**, *21* (4), 1377-1388.
- 113. Visco, I.; Chiantia, S.; Schwille, P., Asymmetric Supported Lipid Bilayer Formation via Methyl-β-Cyclodextrin Mediated Lipid Exchange: Influence of Asymmetry on Lipid Dynamics and Phase Behavior. *Langmuir* **2014**, *30* (25), 7475-7484.
- 114. Robinson, J.; Berselli, G. B.; Ryadnov, M. G.; Keyes, T. E., Annexin V Drives Stabilization of Damaged Asymmetric Phospholipid Bilayers. *Langmuir* **2020**, *36* (19), 5454-5465.
- 115. Shi, X.; Kohram, M.; Zhuang, X.; Smith, A. W., Interactions and Translational Dynamics of Phosphatidylinositol Bisphosphate (PIP2) Lipids in Asymmetric Lipid Bilayers. *Langmuir* **2016**, *32* (7), 1732-1741.
- 116. Nguyen, M. H. L.; DiPasquale, M.; Rickeard, B. W.; Doktorova, M.; Heberle, F. A.; Scott, H. L.; Barrera, F. N.; Taylor, G.; Collier, C. P.; Stanley, C. B.; Katsaras, J.; Marquardt, D., Peptide-Induced Lipid Flip-Flop in Asymmetric Liposomes Measured by Small Angle Neutron Scattering. *Langmuir* **2019**, *35* (36), 11735-11744.
- 117. Milianta, P. J.; Muzzio, M.; Denver, J.; Cawley, G.; Lee, S., Water Permeability across Symmetric and Asymmetric Droplet Interface Bilayers: Interaction of Cholesterol Sulfate with DPhPC. *Langmuir* **2015**, *31* (44), 12187-12196.
- 118. Yasmann, A.; Sukharev, S., Properties of Diphytanoyl Phospholipids at the Air–Water Interface. *Langmuir* **2015**, *31* (1), 350-357.
- 119. Wylie, J. L.; Hatch, G. M.; McClarty, G., Host cell phospholipids are trafficked to and then modified by Chlamydia trachomatis. *J Bacteriol* **1997**, *179* (23), 7233-42.
- 120. Aranda, F. J.; Espuny, M. J.; Marqués, A.; Teruel, J. A.; Manresa, Á.; Ortiz, A., Thermodynamics of the Interaction of a Dirhamnolipid Biosurfactant Secreted by Pseudomonas aeruginosa with Phospholipid Membranes. *Langmuir* **2007**, *23* (5), 2700-2705.

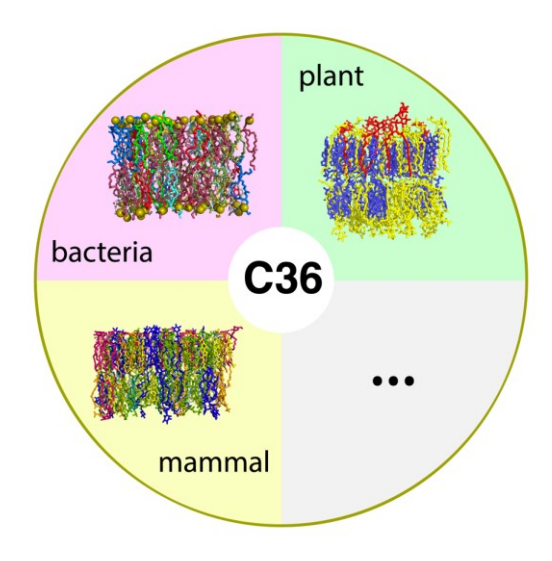
- 121. Marshall, S. E.; Hong, S.-H.; Thet, N. T.; Jenkins, A. T. A., Effect of Lipid and Fatty Acid Composition of Phospholipid Vesicles on Long-Term Stability and Their Response to Staphylococcus aureus and Pseudomonas aeruginosa Supernatants. *Langmuir* **2013**, *29* (23), 6989-6995.
- 122. Stoica, O.; Tuanyok, A.; Yao, X.; Jericho, M. H.; Pink, D.; Beveridge, T. J., Elasticity of Membrane Vesicles Isolated from Pseudomonas aeruginosa. *Langmuir* **2003**, *19* (26), 10916-10924.
- 123. Rahnamoun, A.; Kim, K.; Pedersen, J. A.; Hernandez, R., Ionic Environment Affects Bacterial Lipopolysaccharide Packing and Function. *Langmuir* **2020**, *36* (12), 3149-3158.
- 124. Sharma, P.; Parthasarathi, S.; Patil, N.; Waskar, M.; Raut, J. S.; Puranik, M.; Ayappa, K. G.; Basu, J. K., Assessing Barriers for Antimicrobial Penetration in Complex Asymmetric Bacterial Membranes: A Case Study with Thymol. *Langmuir* **2020**, *36* (30), 8800-8814.
- 125. Clifton, L. A.; Ciesielski, F.; Skoda, M. W. A.; Paracini, N.; Holt, S. A.; Lakey, J. H., The Effect of Lipopolysaccharide Core Oligosaccharide Size on the Electrostatic Binding of Antimicrobial Proteins to Models of the Gram Negative Bacterial Outer Membrane. *Langmuir* **2016**, *32* (14), 3485-3494.
- 126. Clifton, L. A.; Skoda, M. W. A.; Le Brun, A. P.; Ciesielski, F.; Kuzmenko, I.; Holt, S. A.; Lakey, J. H., Effect of Divalent Cation Removal on the Structure of Gram-Negative Bacterial Outer Membrane Models. *Langmuir* **2015**, *31* (1), 404-412.
- 127. Michel, J. P.; Wang, Y. X.; Kiesel, I.; Gerelli, Y.; Rosilio, V., Disruption of Asymmetric Lipid Bilayer Models Mimicking the Outer Membrane of Gram-Negative Bacteria by an Active Plasticin. *Langmuir* **2017**, *33* (41), 11028-11039.
- 128. Lomize, A. L.; Pogozheva, I. D.; Mosberg, H. I., Anisotropic solvent model of the lipid bilayer. 2. Energetics of insertion of small molecules, peptides, and proteins in membranes. *J Chem Inf Model* **2011,** *51* (4), 930-46.
- 129. Furt, F.; Simon-Plas, F.; Mongrand, S., Lipids of the Plant Plasma Membrane. In *The Plant Plasma Membrane*, Murphy, A. S.; Schulz, B.; Peer, W., Eds. Springer Berlin Heidelberg: Berlin, Heidelberg, 2011; pp 3-30.
- 130. Whitman, C. E.; Travis, R. L., Phospholipid Composition of a Plasma Membrane-Enriched Fraction from Developing Soybean Roots. *Plant Physiology* **1985**, *79* (2), 494-498.
- 131. Markham, J. E.; Li, J.; Cahoon, E. B.; Jaworski, J. G., Separation and Identification of Major Plant Sphingolipid Classes from Leaves. *Journal of Biological Chemistry* **2006**, *281* (32), 22684-22694.
- 132. Wenk, M. R., Lipidomics: New Tools and Applications. Cell 2010, 143 (6), 888-895.
- 133. van Eerden, F. J.; de Jong, D. H.; de Vries, A. H.; Wassenaar, T. A.; Marrink, S. J., Characterization of thylakoid lipid membranes from cyanobacteria and higher plants by molecular dynamics simulations. *Biochimica et Biophysica Acta (BBA) Biomembranes* **2015**, *1848* (6), 1319-1330.

- 134. Quan, X.; Peng, C.; Zhao, D.; Li, L.; Fan, J.; Zhou, J., Molecular Understanding of the Penetration of Functionalized Gold Nanoparticles into Asymmetric Membranes. *Langmuir* **2017**, *33* (1), 361-371.
- 135. López Cascales, J. J.; Otero, T. F.; Smith, B. D.; González, C.; Márquez, M., Model of an Asymmetric DPPC/DPPS Membrane: Effect of Asymmetry on the Lipid Properties. A Molecular Dynamics Simulation Study. *The Journal of Physical Chemistry B* **2006**, *110* (5), 2358-2363.
- 136. He, X.; Lin, M.; Sha, B.; Feng, S.; Shi, X.; Qu, Z.; Xu, F., Coarse-grained molecular dynamics studies of the translocation mechanism of polyarginines across asymmetric membrane under tension. *Scientific Reports* **2015**, *5* (1), 12808.
- 137. Polley, A.; Mayor, S.; Rao, M., Bilayer registry in a multicomponent asymmetric membrane: Dependence on lipid composition and chain length. *The Journal of Chemical Physics* **2014**, *141* (6), 064903.
- 138. Yu, Y.; Klauda, J. B., Symmetric and Asymmetric Models for the Arabidopsis thaliana Plasma Membrane: A Simulation Study. *The Journal of Physical Chemistry B* **2021**, *125* (41), 11418-11431.
- 139. Uemura, M.; Joseph, R. A.; Steponkus, P. L., Cold Acclimation of Arabidopsis thaliana (Effect on Plasma Membrane Lipid Composition and Freeze-Induced Lesions). *Plant Physiology* **1995**, *109* (1), 15.
- 140. Hsieh, T. C. Y.; Kaul, K.; Laine, R. A.; Lester, R. L., Structure of a major glycophosphoceramide from tobacco leaves, PSL-I: 2-deoxy-2-acetamido-D-glucopyranosyl(  $\alpha$  1  $\rightarrow$  4)-D-glucuronopyranosyl(  $\alpha$  1  $\rightarrow$  2)myoinositol-1-O-phosphoceramide. *Biochemistry* **1978,** *17* (17), 3575-3581.
- 141. Sodt, A. J.; Sandar, M. L.; Gawrisch, K.; Pastor, R. W.; Lyman, E., The Molecular Structure of the Liquid-Ordered Phase of Lipid Bilayers. *Journal of the American Chemical Society* **2014**, *136* (2), 725-732.
- 142. Marquardt, D.; Geier, B.; Pabst, G., Asymmetric Lipid Membranes: Towards More Realistic Model Systems. *Membranes* **2015**, *5* (2), 180-196.
- 143. Markones, M.; Drechsler, C.; Kaiser, M.; Kalie, L.; Heerklotz, H.; Fiedler, S., Engineering Asymmetric Lipid Vesicles: Accurate and Convenient Control of the Outer Leaflet Lipid Composition. *Langmuir* **2018**, *34* (5), 1999-2005.
- 144. Adams, M.; Wang, E.; Zhuang, X.; Klauda, J. B., Simulations of simple Bovine and Homo sapiens outer cortex ocular lens membrane models with a majority concentration of cholesterol. *Biochimica et Biophysica Acta (BBA) Biomembranes* **2018**, *1860* (10), 2134-2144.

- 145. Wang, E.; Klauda, J. B., Models for the Stratum Corneum Lipid Matrix: Effects of Ceramide Concentration, Ceramide Hydroxylation, and Free Fatty Acid Protonation. *J Phys Chem B* **2018**, *122* (50), 11996-12008.
- 146. Wang, E.; Klauda, J. B., Molecular Structure of the Long Periodicity Phase in the Stratum Corneum. *Journal of the American Chemical Society* **2019**, *141* (42), 16930-16943.
- 147. Yuan, Y.; Yu, Y.; Klauda, J. B., Simulations of Diabetic and Non-Diabetic Peripheral Nerve Myelin Lipid Bilayers. *The Journal of Physical Chemistry B* **2021**, *125* (23), 6201-6213.
- 148. Beddoes, C. M.; Gooris, G. S.; Foglia, F.; Ahmadi, D.; Barlow, D. J.; Lawrence, M. J.; Demé, B.; Bouwstra, J. A., Arrangement of Ceramides in the Skin: Sphingosine Chains Localize at a Single Position in Stratum Corneum Lipid Matrix Models. *Langmuir* **2020**, *36* (34), 10270-10278.
- 149. Bouwstra, J.; Gooris, G.; Ponec, M., The Lipid Organisation of the Skin Barrier: Liquid and Crystalline Domains Coexist in Lamellar Phases. *Journal of Biological Physics* **2002**, *28* (2), 211-223.
- 150. McIntosh, T. J., Organization of Skin Stratum Corneum Extracellular Lamellae: Diffraction Evidence for Asymmetric Distribution of Cholesterol. *Biophysical Journal* **2003**, *85* (3), 1675-1681.
- 151. Harding, C. R., The stratum corneum: structure and function in health and disease. *Dermatologic Therapy* **2004**, *17* (s1), 6-15.
- 152. Wang, E.; Klauda, J. B., Simulations of Pure Ceramide and Ternary Lipid Mixtures as Simple Interior Stratum Corneum Models. *The Journal of Physical Chemistry B* **2018**, *122* (10), 2757-2768.
- 153. Gupta, R.; Rai, B., Molecular Dynamics Simulation Study of Skin Lipids: Effects of the Molar Ratio of Individual Components over a Wide Temperature Range. *The Journal of Physical Chemistry B* **2015**, *119* (35), 11643-11655.
- 154. Das, C.; Noro, M. G.; Olmsted, P. D., Simulation studies of stratum corneum lipid mixtures. *Biophysical Journal* **2009**, *97* (7), 1941-1951.
- 155. Das, C.; Olmsted, P. D., The physics of stratum corneum lipid membranes. *Philosophical Transactions of the Royal Society A: Mathematical, Physical and Engineering Sciences* **2016,** *374* (2072), 20150126.
- 156. MacDermaid, C. M.; DeVane, R. H.; Klein, M. L.; Fiorin, G., Dehydration of multilamellar fatty acid membranes: Towards a computational model of the stratum corneum. *The Journal of Chemical Physics* **2014**, *141* (22), 22D526.
- 157. Groen, D.; Gooris, G. S.; Barlow, D. J.; Lawrence, M. J.; van Mechelen, J. B.; Demé, B.; Bouwstra, J. A., Disposition of Ceramide in Model Lipid Membranes Determined by Neutron Diffraction. *Biophysical Journal* **2011**, *100* (6), 1481-1489.
- 158. Bunge, R. P., Glial cells and the central myelin sheath. *Physiological Reviews* **1968**, *48* (1), 197-251.

- 159. Zuvic-Butorac, M.; Kriz, J.; Simonic, A.; Schara, M., Fluidity of the myelin sheath in the peripheral nerves of diabetic rats. *Biochimica et Biophysica Acta (BBA) Molecular Basis of Disease* **2001,** *1537* (2), 110-116.
- 160. Sinnreich, M.; Taylor, B. V.; Dyck, P. J., Diabetic neuropathies. Classification, clinical features, and pathophysiological basis. *Neurologist* **2005**, *11* (2), 63-79.
- 161. Sugimoto, K.; Murakawa, Y.; Sima, A. A. F., Diabetic neuropathy a continuing enigma. *Diabetes/Metabolism Research and Reviews* **2000**, *16* (6), 408-433.

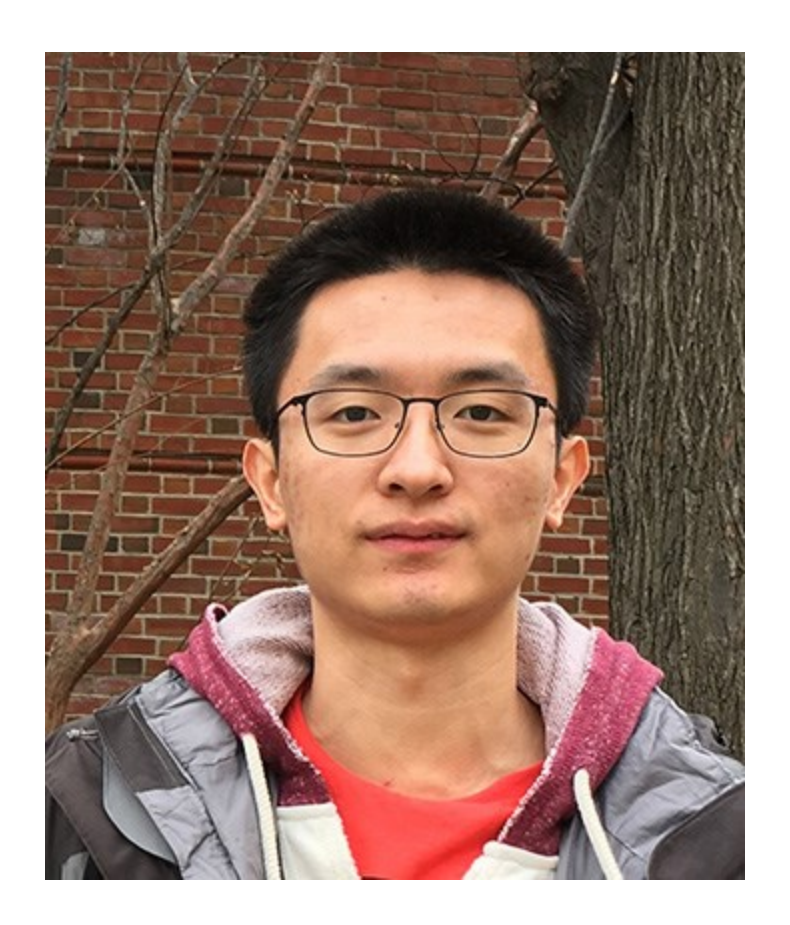
# **TOC GRAPHIC**



# **Biographies**



Min-Kang Hsieh is a postdoctorial associate at the University of Maryland where he investigates complex membranes in bacteria and membrane-accessory proteins interactions in SARS-CoV-2 virus, guided by Dr. Jeffery Klauda. He received his Ph. D. in Chemical Engineering at Columbia University where he developed a novel fluorescent labeling nucleotide for DNA sequencing technology.



Yalun Yu is a Ph. D. candidate in the Biophysics Program at the University of Maryland where, with guidance from co-advisors Jeffery Klauda and Richard Pastor (NIH), he uses MD simulations to investigate complex membranes such as those of plants and bacteria. He also focuses on lipid force field parameterization (additive and polarizable). Recent publications include adding the long-range dispersion into the C36 additive lipid FF (C36/LJ-PME) and update of the C36UA model for acyl chain.



Professor Jeffery Klauda received a B.S. in Chemical Engineering and Applied Mathematics from Rensselaer Polytechnic Institute in 1998. His Ph.D. research (1998-2003) was done at the University of Delaware under the advisement of Prof. Stanley Sandler focusing on thermodynamic modeling of gas hydrates, gas adsorption on nanoporous carbons, and quantum mechanical studies of adsorption. He switched his research focus to biological areas and molecular simulation during his postdoctoral fellowship at the National Institutes of Health in the National Heart, Lung and Blood Institute (NHLBI) under the advisement of Drs. Bernie Brooks and Rich Pastor (2003-2007). In 2007, he joined as a tenure-track professor in the Department of Chemical and Biomolecular Engineering at the University of Maryland – College Park. He is currently a Full Professor and is the Associate Chair/Director of Graduate Studies in the Department of Chemical and Biomolecular Engineering and the co-Director of the Biophysics Program.